18 Heavy quarks and leptons

The top quark is the only known fundamental fermion with a mass on the electroweak scale. As a result, study of the top quark may provide an excellent probe of the sector of electroweak symmetry breaking (EWSB), and new physics may well be discovered in either its production or decay. The LHC will be a 'top quark factory', and a very large variety of top physics studies will be possible with the high statistics samples which will be accumulated.

Figure 18-1 shows the expected cross-section for the pair production of heavy quarks at the LHC for quark masses in the range from 175 to 1000 GeV. For the case of the top quark, with $m_t \approx 175$ GeV, the next-to-leading order (NLO) prediction including gluon resummation is $\sigma(t\bar{t}) = 833$ pb [18-1]. In addition to the detailed studies of top quark physics which this large cross-section will allow, the LHC will be an excellent place to search for the possible existence of fourth generation quarks and leptons. Approximately 1000 events would be produced per low luminosity year for a quark mass of 900 GeV.

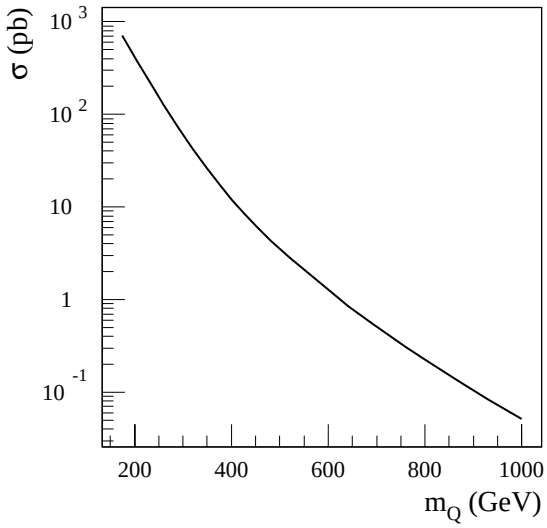

Figure 18-1 Predicted Standard Model cross-section, versus quark mass, for pair production of heavy quarks at the LHC.

Section 18.1 discusses the ATLAS sensitivity to many topics related to top quark physics. Section 18.2 presents the ATLAS discovery potential for fourth generation quarks, and Section 18.3 briefly develops ideas on searching for heavy leptons.

The results presented in this chapter are obtained predominantly using ATLFAST [18-2], the parametrised ATLAS detector simulation (see Section 2.5). Cross-checks of the results, particularly for the case of the measurement of the top quark mass, have been made using the detailed GEANT simulation of the ATLAS detector.

18.1 Top quark physics

18.1.1 Introduction

With the discovery of the top quark at Fermilab [18-3][18-4], top physics has moved from the search phase into the study phase. The NLO prediction that $\sigma(t\bar{t}) = 833$ pb at the LHC [18-1] implies production of more than 8 million $t\bar{t}$ pairs per year at low luminosity (and, of course, ten times that number per year at high luminosity). The motivations for detailed studies of the top quark are numerous. Within the Standard Model (SM), an accurate measurement of the top quark mass (m_t) helps constrain the mass of the SM Higgs boson (m_H). The large value of m_t implies the top quark may provide an excellent probe of EWSB, fermion mass generation, and the possible existence of other massive particles. In addition, top quark events will be the dominant background in many searches for new physics at the TeV scale; extraction of new physics will

therefore require detailed measurement and understanding of the production rate and properties of top quark events. Also, the $W \rightarrow jj$ decays in top quark events provide an important *in situ* calibration source for calorimetry at the LHC (see Section 9.3.1 and Section 12.5).

The next section describes briefly the kinematics of $t\bar{t}$ events at the LHC, and presents estimates of the event samples which will be accumulated. Section 18.1.3 discusses in detail the estimated precision which can be achieved in the measurement of the mass of the top quark, one of the fundamental parameters of the SM. In Section 18.1.4, studies of $t\bar{t}$ production are presented. Section 18.1.5 then presents results related to top quark decays and couplings. Finally, Section 18.1.6 describes studies of electroweak single top production, and of the variety of physics topics which can be best (or only) studied using this channel.

Apart from the analyses of single top production, where a variety of Monte Carlo signal generators have been used (see Section 18.1.6 for details), top quark signal processes have been simulated with the PYTHIA Monte Carlo program [18-5], including initial- and final-state radiation, hadronisation and decays. Most background processes have also been generated with PYTHIA, with the exception of $Wb\bar{b}$, which has been produced using HERWIG [18-6], where the correct matrix-element calculation of that process is available. For most top physics analyses, the backgrounds from non-top final states are small after selection cuts and the remaining background is dominated by top events themselves. Therefore, unlike most of the other chapters in the TDR which use leading-order (LO) predictions for cross-sections since NLO predictions are not available for all the relevant backgrounds, the top quark analyses use the NLO prediction that $\sigma(t\bar{t}) = 833$ pb. All analyses assumed efficiencies for charged lepton reconstruction and identification of 90%.

18.1.2 $t\bar{t}$ selection and event yields

At the LHC, the largest source of top quarks is from $t\bar{t}$ production. According to the SM, the top quark decays almost exclusively to Wb. The final state topology of $t\bar{t}$ events then depends on the decay modes of the W bosons. In approximately 65.5% of $t\bar{t}$ events, both W bosons decay hadronically via $W \rightarrow jj$, or at least one W decays via $W \rightarrow \tau\nu$. These events are difficult to extract cleanly above the large QCD multi-jet background, and are for the most part not considered further. Instead, the analyses presented here concentrate on 'leptonic $t\bar{t}$ events', where at least one of the W bosons decays via $W \rightarrow l\nu$ (with the charged lepton either an electron or muon). The lepton plus large $E_{\mathrm{T}}^{\mathrm{miss}}$, due to the escaping neutrino(s), provide a large suppression against multi-jet backgrounds. The leptonic events, which account for approximately 34.5% of all $t\bar{t}$ events, can be subdivided into a 'single lepton plus jets' sample and a 'dilepton' sample, depending on whether one or both W bosons decay leptonically.

18.1.2.1 Single lepton plus jets sample

The single lepton plus jets topology, where one W decays leptonically and the other W decays hadronically via $W \rightarrow jj$, arises in $2 \times 2/9 \times 6/9 \approx 29.6\%$ of all $t\bar{t}$ events. One expects, therefore, production of almost 2.5 million single lepton plus jet events for an integrated luminosity of 10 fb^{-1}. The presence of a high p_{T} isolated electron or muon allows these events to be triggered efficiently, using, for example, the single lepton triggers discussed in Section 11.7.3. Furthermore, the complete final state can be reconstructed (with a quadratic ambiguity), despite the missing neutrino, by assuming $E_{\mathrm{T}}^{\mathrm{miss}} = E_{\mathrm{T}}(\nu)$ and applying the constraint that $m_{l\nu} = m_W$.

An important tool for selecting clean top quark samples, particularly in the single lepton plus jets mode, is the ability to identify *b*-quarks. As discussed in detail in Chapter 10, with a tagging efficiency of 60% for *b*-jets, a rejection of at least 100 can be achieved against prompt jets (*i.e.* jets containing no long-lived particles) at low luminosity. At high luminosity, a rejection factor of around 100 is obtained with a reduced *b*-tagging efficiency of 50%.

Requiring an isolated lepton with p_T > 20 GeV, E_T^{miss} > 20 GeV, and at least four jets with p_T > 20 GeV, including at least one *b*-tagged jet, a sample of about 820 000 single *b*-tagged events would be selected for an integrated luminosity of 10 fb^{-1}. Figure 18-2 and Figure 18-3 show the p_T(lepton) and jet multiplicity distribution for events with p_T(lepton) > 20 GeV, normalised to an integrated luminosity of 10 fb^{-1}. For the jets distribution a p_T(jet) > 20 GeV has been required.

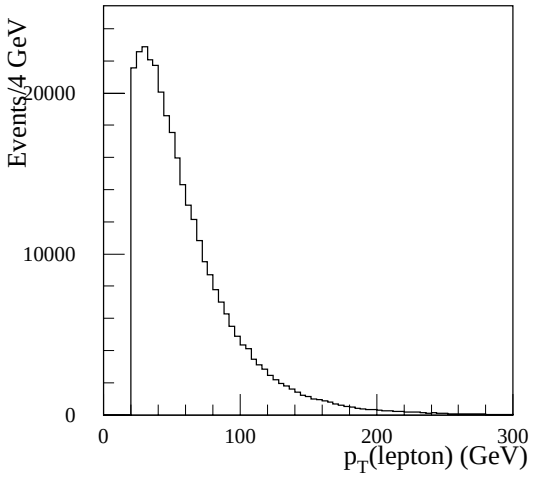

Figure 18-2 p_T(lepton) distribution for single lepton plus jet events with a lepton p_T > 20 GeV, normalised to an integrated luminosity of 10 fb^{-1}.

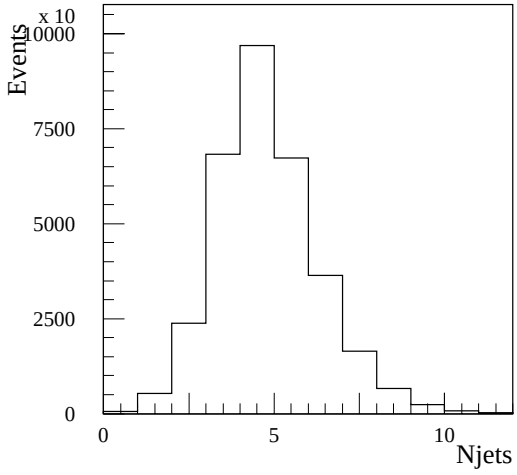

Figure 18-3 Distribution of jet multiplicity (threshold at p_T > 20 GeV) for single lepton plus jet events with a lepton p_T > 20 GeV, normalised to an integrated luminosity of 10 fb^{-1}.

18.1.2.2 Dilepton sample

Dilepton events, where each *W* decays leptonically, provide a particularly clean sample of $t\bar{t}$ events, although the product of branching ratios is small, 2/9 x 2/9 ≈ 4.9%. With this branching ratio, one expects the production of over 400 000 dilepton events for an integrated luminosity of 10 fb^{-1}. The presence of two high p_T isolated leptons allows these events to be triggered efficiently, using the single or double lepton triggers discussed in Section 11.7.3.

18.1.2.3 multi-jet sample

The largest sample of $t\bar{t}$ events consists of six-jet events from the fully hadronic decay mode, $t\bar{t} \rightarrow WWb\bar{b} \rightarrow (jj)(jj)b\bar{b}$. With a branching ratio of 6/9 x 6/9 ≈ 44.4%, it corresponds to the production of 3.7 million multi-jet events for an integrated luminosity of 10 fb^{-1}. However, these events suffer from a very large background from QCD multi-jet events. In addition, the all-jet final state poses difficulties for triggering. The trigger menus discussed in Section 11.7.3 consider

multi-jet trigger thresholds only up to four jets, for which a jet E_T threshold of 55 GeV is applied at low luminosity. Further study is required to determine appropriate thresholds for a six-jet topology.

A very preliminary investigation [18-7] has been made of a simple selection and reconstruction algorithm for attempting to extract the multi-jet $t\bar{t}$ signal from the background. Hadronic $t\bar{t} \rightarrow WWb\bar{b} \rightarrow (jj)(jj)b\bar{b}$ events were selected by requiring six or more jets with $p_T > 15$ GeV, with at least two of them tagged as b-jets. Jets were required to satisfy $|\eta| < 3$ ($|\eta| < 2.5$ for b-jet candidates). In addition, the scalar sum of the transverse momenta of the jets was required to be greater than 200 GeV. The $t\bar{t}$ signal efficiency for these cuts was 19.3%, while only 0.29% of 1.8 million QCD multi-jet events survived. With this selection, and assuming a QCD multi-jet cross-section of 1.4×10^{-3} mb for p_T(hard process) > 100 GeV, one obtains a signal-to-background ratio S / B ≈ 1 / 57.

Reconstruction of the $t\bar{t}$ final state proceeded by first selecting di-jet pairs, from among those jets not tagged as b-jets, to form $W \rightarrow jj$ candidates. A χ^2_W was calculated from the deviations of the two m_{jj} values from the known value of m_W. The combination which minimised the value of χ^2_W was selected, and events with $\chi^2_W > 3.5$ were rejected. For accepted events, the two W candidates were then combined with b-tagged jets to form top and anti-top quark candidates, and a χ^2_t calculated as the deviation from the condition that the top and anti-top masses are equal. Again, the combination with the lowest χ^2_t was selected, and events with $\chi^2_t > 7$ were rejected. After this reconstruction procedure and cuts, the value of S / B improved to 1 / 8 within the mass window 130-200 GeV, or slightly better for higher p_T(jet) thresholds (see Table 18-1).

Table 18-1 For different p_T(jet) thresholds, the efficiency of the selection cuts and reconstruction algorithm described in the text, for the $t\bar{t}$ multi-jet signal and the background from QCD multi-jets. Also included is the resulting ratio of $t\bar{t}$ signal to QCD background (S/B) within a mass window $130 < m_{jjb} < 200$ GeV.

p_T(jet) threshold	Signal (%)	QCD (%)	S/B
15 GeV	7.2	.028	1 / 8
20 GeV	4.3	.014	1 / 7
25 GeV	2.5	.0056	1 / 6

The isolation of a top signal can be further improved in a number of ways, such as using a multivariate discriminant based on kinematic variables like aplanarity, sphericity or ΔR(jet-jet), or restricting the analysis to a sample of high p_T top events. These techniques are undergoing further investigation, but it will be very difficult to reliably extract the signal from the background in this channel. In particular, the multi-jet rates and topologies, as generated by PYTHIA, suffer from very large uncertainties. Comparisons with the NJETS [18-8] matrix-element calculations have shown [18-9] that these uncertainties are about a factor of three for three- or four-jet final states. In the case of six-jet final states, the uncertainties could be expected to be even larger.

18.1.3 Measurement of the top quark mass

The most recent combined value of the top quark mass from CDF and D0 is $m_t = 174.3 \pm 3.2 \pm 4.0$ GeV [18-10]. The mass of the top quark is a fundamental parameter of the SM and should be measured as accurately as possible. As is well known, radiative corrections in the SM relate the mass of the top quark and the mass of the W to the mass of the SM Higgs boson. Assuming that m_W can be measured with a precision of ±20 MeV (see Section 16.1), a determination of m_t with a precision of $\delta m_t \leq \pm 2$ GeV would be required to match that from m_W and from the current theoretical uncertainties. Models beyond the SM which attempt to explain in a

more fundamental way the origin of mass and the observed fermion mass hierarchy, such as top-bottom-tau Yukawa coupling unification in a supersymmetric SO(10) GUT [18-11], would profit from a precision of the order $\delta m_t \approx \pm 1$ GeV.

With the large number of top quark events which will be available at the LHC, the uncertainty in the measurement of m_t will be dominated by systematic errors. Several different data samples and methods, with somewhat differing sensitivities to systematic errors, can be used, and the resulting measurements can then be combined for optimal precision.

The studies presented in this section were performed predominantly using ATLFAST [18-2], since they concentrated on the influence on the m_t measurement of various 'physics-related' sources of uncertainties, such as initial and final state radiation, and uncertainties in the knowledge of *b*-quark fragmentation. As discussed in Section 18.1.3.5, some cross-checks of the results have been made with results from a detailed GEANT simulation of the ATLAS detector. However, detailed studies of 'detector-related' effects, and in particular of the calibration and understanding of the jet energy scale, are not discussed here, but in Chapter 9 and Chapter 12. The top mass measurement is assumed to be performed using data taken during low luminosity running, and so pile-up has not been included. Detector noise is also not included, but should not significantly affect the results.

18.1.3.1 Inclusive single lepton plus jets channel

The process $pp \rightarrow t\bar{t} \rightarrow WWb\bar{b} \rightarrow (l\nu)(jj)b\bar{b}$ provides a large sample of top quark events. The presence of a high p_T isolated lepton provides an efficient trigger. The lepton and the high value of E_T^{miss} give a large suppression of backgrounds from QCD multi-jets and $b\bar{b}$ production. The major sources of backgrounds are W+jet production with $W \rightarrow l\nu$ decay, and Z+jet events with $Z \rightarrow ll$. Potential backgrounds from WW, WZ, and ZZ gauge boson pair production have also been studied, but are reduced to a negligible level after cuts.

For the single lepton plus jets sample, it is possible to fully reconstruct the $t\bar{t} \rightarrow WWb\bar{b} \rightarrow (l\nu)(jj)b\bar{b}$ final state. The four-momentum of the missing neutrino can be reconstructed by setting $m_\nu = 0$, assigning $E_T(\nu) = E_T^{miss}$, and calculating $p_z(\nu)$, with a quadratic ambiguity, by applying the constraint that $m_{l\nu} = m_W$. If one applies the further kinematic constraints that $m_{jj} = m_W$ and $m_{jjb} = m_{l\nu b} = m_t$, the top mass can be determined using a three-constraint fit. This kinematic fit technique currently gives the most precise determination of m_t at the Tevatron [18-12], where statistics are limited. However, if the systematic errors are to be kept small, this method requires an excellent modelling and understanding of the E_T^{miss} distribution and resolution, which is beyond the scope of the studies reported here. The discussion presented here (for more details, see [18-13]) will focus on the method where the isolated lepton and large E_T^{miss} are used to tag the event, and the value of m_t is extracted as the invariant mass of the three jet system arising from the hadronic top quark decay (*i.e.* $m_t = m_{jjb}$).

Events were selected by requiring an isolated lepton with $p_T > 20$ GeV and $|\eta| < 2.5$, and $E_T^{miss} > 20$ GeV. Jets were reconstructed using a fixed cone algorithm. Cone sizes of $\Delta R = 0.4$ and 0.7 were investigated. At least four jets with $p_T > 40$ GeV and $|\eta| < 2.5$ were required, and at least two of the jets were required to be tagged as *b*-jets. In Table 18-2, the selection efficiencies for the signal and background processes after each successive cut are presented, together with the expected S/B ratio.

For an integrated luminosity of 10 fb^{-1}, a signal of 126 000 $t\bar{t}$ events was obtained after selection cuts, with a small background of 1,922 events, yielding a value of S/B = 65.

Table 18-2 Efficiencies (in percent), not including branching ratios, for the inclusive $t\bar{t}$ single lepton plus jets signal and for background processes, as a function of the selection cuts applied. The last column gives the equivalent number of events for an integrated luminosity of 10 fb^{-1}, and the signal-to-background ratio.

Process	p_T^l > 20GeV E_T^{miss} > 20GeV	As before, plus $N_{jet} \geq 4$	As before, plus $N_{b\text{-}jet} \geq 2$	Events per 10 fb^{-1}
$t\bar{t}$ signal	64.7	21.2	5.0	126 000
W+jets	47.9	0.1	0.002	1658
Z+jets	15.0	0.05	0.002	232
WW	53.6	0.5	0.006	10
WZ	53.8	0.5	0.02	8
ZZ	2.8	0.04	0.008	14
Total background				1922
S/B				65

For accepted events, the decay $W \rightarrow jj$ was reconstructed from among those jets that were not tagged as b-jets. The jet pair with an invariant mass m_{jj} closest to m_W was selected as the W candidate. The invariant mass distribution of the selected di-jet combinations is shown in Figure 18-4. Fitting the distribution with a Gaussian plus a third order polynomial yielded a W mass consistent with the generated value and a m_{jj} mass resolution of 7.8 GeV. Within a mass window of ±20 GeV around m_W, the purity (P) and efficiency (ε) of the W reconstruction, determined by comparing with the parton level information, were P = 67% and ε = 90%, respectively. The background is dominated by wrong combinations in the $t\bar{t}$ events themselves. Other selection criteria, such as requiring that the highest p_T jet be part of the combination, did not improve significantly the purity nor efficiency, and therefore are not considered in the following.

Events with $|m_{jj} - m_W| < 20$ GeV were retained, and the W candidate was then combined with one of the b-tagged jets to attempt to reconstruct $t \rightarrow Wb$. If one does not do anything to choose between the b-tagged jets, one reconstructs at least two jjb combinations per event. In this case, the right combination is always selected but the purity is only 30%. To choose the correct jjb combination, a variety of criteria were tried, including choosing the jjb combination which gave the highest p_T for the reconstructed top candidate, or using the b-jet which was furthest from the isolated lepton. Similar results were obtained for these various methods. Figure 18-5 presents the reconstructed m_{jjb} distribution using the jjb combination which gives the highest p_T for the reconstructed top candidate. Fitting the distribution with a Gaussian plus a third order polynomial yielded a top mass consistent with the generated value of 175 GeV, and a m_{jjb} mass resolution of 11.9 GeV.

Normalising to an integrated luminosity of 10 fb^{-1}, about 32 000 signal events were reconstructed, of which 30 000 yielded a value of m_{jjb} within a window of ±35 GeV around the generated value of m_t = 175 GeV. In addition, 34 000 'wrong combinations' in $t\bar{t}$ events were obtained (where the incorrect jet-parton assignment was made), of which 14 000 were in the mass window around m_t. The total background from processes other than $t\bar{t}$ summed up to only 115 events. In the mass window defined above, the signal purity and overall efficiency were P = 68% and ε = 69%, respectively. The determination of m_t by fitting the peak in the measured m_{jjb} spectrum resulted in a statistical uncertainty of δm_t(stat.) = ±0.070 GeV for an integrated luminosity of 10 fb^{-1}.

Performing the same analysis, but relaxing the *b*-tagging criterion to require at least one *b*-jet, yielded 80 000 signal events, with 76 000 having m_{jjb} within a window of ±35 GeV around the generated value of m_t = 175 GeV. In addition, 166 000 wrong $t\bar{t}$ combinations were accepted, with 58 000 in the mass window, and 6 000 events from other background processes. The resultant statistical error on m_t was reduced to δm_t(stat.) = ±0.042 GeV.

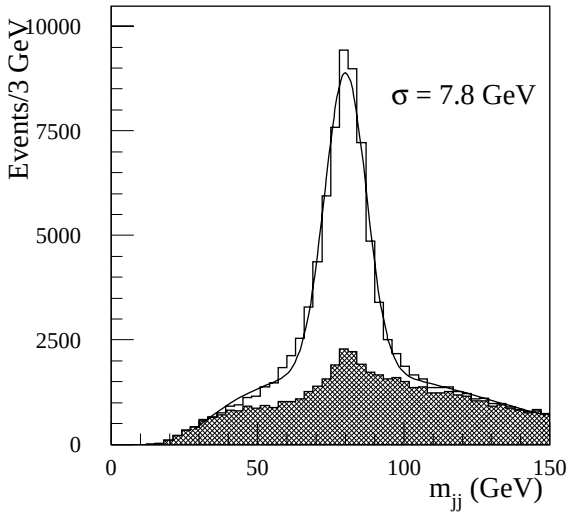

Figure 18-4 Invariant mass distribution of the selected *jj* pairs for the inclusive sample, normalised to an integrated luminosity of 10 fb^{-1}. The shaded histogram shows the background, which is dominated by 'wrong combinations' from $t\bar{t}$ events.

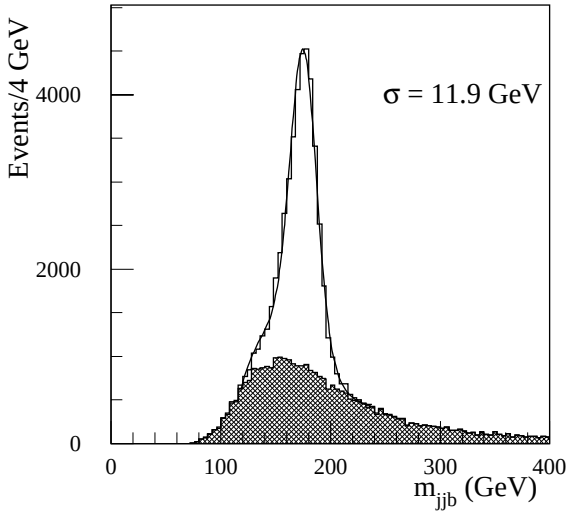

Figure 18-5 Invariant mass distribution of the accepted *jjb* combinations for the inclusive sample, normalised to an integrated luminosity of 10 fb^{-1}. The shaded histogram shows the background, which is dominated by 'wrong combinations' from $t\bar{t}$ events. Only the *jjb* combination with the highest p_T is shown for each event.

The dependence of the reconstructed top mass on the generated value was checked using several samples of $t\bar{t}$ events with different values of m_t ranging from 160 to 190 GeV. The results are shown in Figure 18-6, and demonstrate a linear dependence of the reconstructed value of m_t on the generated top mass. The stability of the reconstructed value of m_t was also checked as a function of p_T(top). As shown in Figure 18-7, no significant p_T(top) dependence was observed. The systematic errors on the measurement of m_t are discussed in Section 18.1.3.3.

18.1.3.2 High p_T single lepton plus jets channel

At the LHC, the $t\bar{t}$ production rate is sufficiently large that one can make very tight cuts and still accept a sample of events for which the statistical error on m_t will be small compared to the systematic error. One could, for example, require that the top and anti-top quarks have high p_T. In this case, they would be produced back-to-back, and the daughters from the two top decays would appear in distinct 'hemispheres' of the detector. This topology would greatly reduce the combinatorial background from having to select which jets have to be combined to reconstruct the $t \rightarrow jjb$ candidate. Backgrounds from processes other than $t\bar{t}$ would also be reduced at high p_T. Furthermore, the higher average energy of the jets to be reconstructed should reduce the sensitivity to systematic effects due to the jet energy calibration and to effects of gluon radiation.

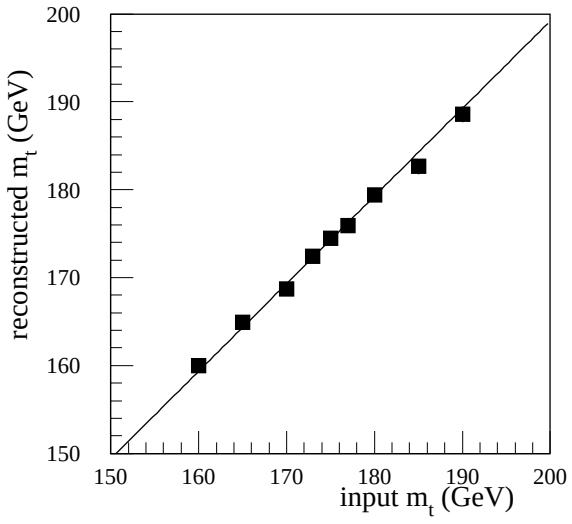

Figure 18-6 Dependence of the reconstructed value of m_t on the generated value of m_t for the inclusive single lepton plus jets sample.

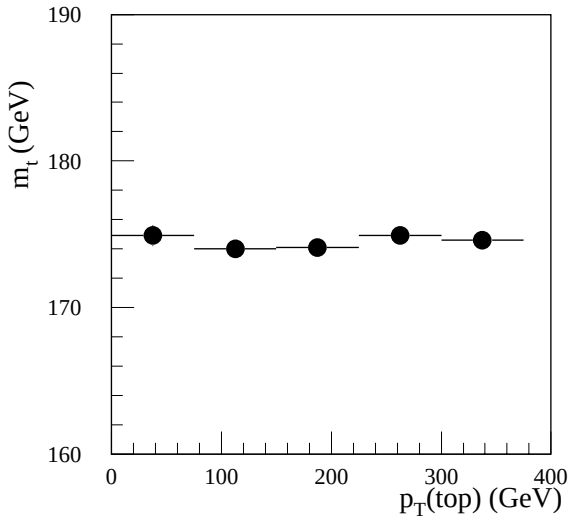

Figure 18-7 Dependence of the reconstructed value of m_t on the generated value of p_T(top) for the inclusive single lepton plus jets sample.

High p_T $t\bar{t}$ events were generated using PYTHIA 5.7 with a p_T cut on the hard scattering process above 200 GeV. The expected cross-section in this case is about 120 pb, or about 14.5% of the total $t\bar{t}$ production cross-section. The selection cuts required the presence of an isolated lepton with $p_T > 30$ GeV and $|\eta| < 2.5$, and $E_T^{miss} > 30$ GeV. The total transverse energy of the event was required to be greater than 450 GeV. Jets were reconstructed using a cone algorithm with radius $\Delta R = 0.4$.

The plane perpendicular to the direction of the isolated lepton was used to divide the detector into two hemispheres. Considering only jets with $p_T > 40$ GeV and $|\eta| < 2.5$, the cuts required one *b*-tagged jet in the same hemisphere as the lepton, and three jets, one of which was *b*-tagged, in the opposite hemisphere. Di-jet candidates for the $W \rightarrow jj$ decay were selected from among those jets in the hemisphere opposite to the lepton which were not tagged as jets. The resultant m_{jj} invariant mass distribution is shown in Figure 18-8. Fitting the six bins around the peak of the mass distribution with a Gaussian, yielded a W mass consistent with the generated value, and a m_{jj} resolution of 7 GeV, in good agreement with that obtained for the inclusive sample in Figure 18-4.

Di-jets with 40 GeV < m_{jj} < 120 GeV were then combined with the *b*-tagged jet from the hemisphere opposite to the lepton to form $t \rightarrow jjb$ candidates. Finally, the high p_T(top) requirement was imposed by requiring $p_T(jjb) > 250$ GeV. With these cuts, the overall signal efficiency was 1.7%. Background from sources other than $t\bar{t}$ was reduced to a negligible level. The invariant mass distribution of the accepted *jjb* combinations is shown in Figure 18-9. Fitting the six bins around the peak of the mass distribution with a Gaussian, yielded a top mass consistent with the generated value of 175 GeV, and a m_{jjb} mass resolution of 11.8 GeV, in good agreement with that obtained for the inclusive sample in Figure 18-5. For an integrated luminosity of 10 fb^{-1}, a sample of 6 300 events would be collected, leading to a statistical error of δm_t(stat.) = ±0.25 GeV, which remains well below the systematic uncertainty (see Section 18.1.3.3).

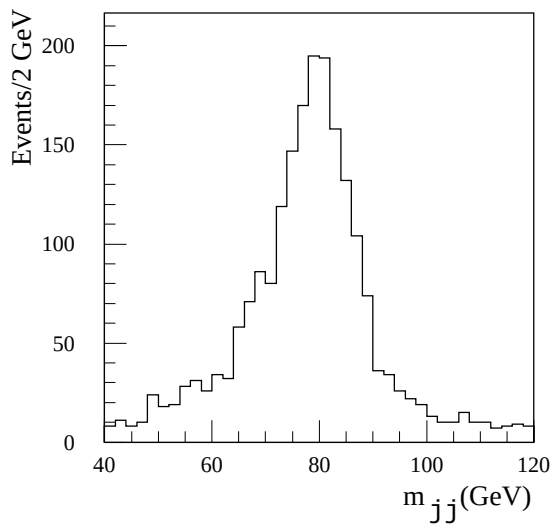

Figure 18-8 Invariant mass distribution of the selected di-jet combinations for the high p_T(top) sample, normalised to an integrated luminosity of 10 fb^{-1}.

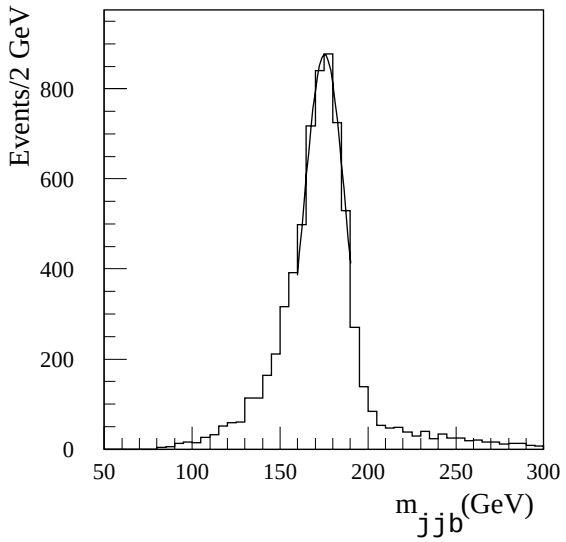

Figure 18-9 Invariant mass distribution of the accepted combinations for the high p_T(top) sample, normalised to an integrated luminosity of 10 fb^{-1}.

Three Monte Carlo data sets, with top masses of 170, 175 and 180 GeV, were used to verify that the reconstructed top mass depends linearly on the Monte Carlo input value. As a stability check of the measurement and of the calibration procedure, the reconstructed value of m_t was determined as a function of $p_T(jjb)$ for the data set with input value m_t = 175 GeV. As in the inclusive sample, no strong p_T dependence was observed.

18.1.3.3 Systematic uncertainties on the measurement of m_t in the single lepton plus jets channel

As discussed below, a number of sources of systematic error on the measurement of m_t using the single lepton plus jets channel have been studied using samples of events generated with PYTHIA and simulated with ATLFAST. In addition, over 60 000 signal events were simulated through the GEANT-based full simulation to allow cross-checks of the ATLFAST results. The results of these comparisons are presented following the discussion of the systematic errors.

The measurement of m_t via reconstruction of $t \rightarrow jjb$ relies on a precise knowledge of the energy calibration for both light quark jets and *b*-jets. The jet energy scale depends on a variety of detector and physics effects, including non-linearities in the calorimeter response, energy lost outside the jet cone (due, for example, to energy swept away by the magnetic field or to gluon radiation at large angles with respect to the original parton), energy losses due to detector effects (cracks, leakage, *etc.*), and 'noise' due to the underlying event. As discussed in Section 9.1 and Section 12.5, the goal is to understand the jet energy scale at the level of 1% for both light quark jets and *b*-jets.

The energy scale of *b*-jets enters in a direct way into the measurement of m_t and must be calibrated from other sources. In contrast, the energy of the two light quark jets can be calibrated event-by-event using the constraint that $m_{jj} = m_W$, at least for the inclusive single lepton plus jets sample, where the jets tend to be well separated. Indeed, the $W \rightarrow jj$ decays in $t\bar{t}$ events provide an essential *in situ* calibration tool for the ATLAS calorimetry system. For the high p_T(top) sample, the two light quark jets from the *W* decay tend to be very close to each other. The ener-

gy sharing between the two jets due to their spatial proximity in the detector complicates the calibration using the m_W constraint, as discussed in Section 9.3.1. A systematic error for the high p_T(top) sample based on the assumption that the W mass constraint cannot be used to perform an event-by-event calibration, is conservatively assumed in the following.

To estimate the effect of an absolute jet energy scale uncertainty, different 'miscalibration' coefficients were applied to the measured jet energies. Effects due to miscalibration of light quark jets and of b-jets were studied separately, and a top mass shift per percent of miscalibration was determined in each case. For example, Figure 18-10 demonstrates the observed linear dependence of the top mass shift on the b-jet absolute scale error for the inclusive sample. Table 18-3 summarises the systematic errors on m_t, defined as the top mass shifts resulting from assumed 1% jet scale errors.

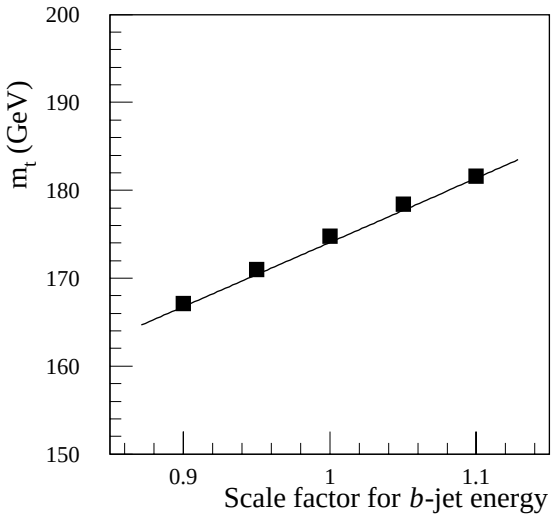

Figure 18-10 Reconstructed top mass for the inclusive single lepton plus jets $t\bar{t}$ sample, as a function of the systematic uncertainty on the energy scale for b-jets.

The fraction of the original b-quark momentum which will appear as visible energy in the reconstruction cone of the corresponding b-jet depends on the fragmentation function of the b-quark. This function is usually parametrised in PYTHIA in terms of one variable, ε_b, using the Peterson fragmentation function [18-14]. The experimental uncertainty on ε_b used here is 0.0025 [18-15]. The value of ε_b usually used in the simulations was ε_b = -0.006. Another sample of signal events was generated with ε_b = (-0.006+0.0025) = -0.0035. The difference between the values of m_t determined with these two samples was taken as the systematic error, $\delta m_t(\varepsilon_b)$, due to uncertainties in the knowledge of ε_b.The resultant systematic uncertainties are summarised in Table 18-3 for the inclusive sample and the high p_T(top) sample.

The presence of initial state radiation (ISR) and final state radiation (FSR) can impact the measurement of m_t. A top mass shift due to ISR, Δm_t(ISR), was defined as the difference between the value of m_t determined for the usual data set with ISR switched on, and the value measured using a sample of events generated with ISR switched off. A similar definition was used to define a shift due to FSR, Δm_t(FSR). In the case of FSR a large mass shift occurs, of order 10 GeV for a jet cone size of ΔR = 0.4. As expected, this large shift is considerably reduced if the cone size to reconstruct the jet is increased to ΔR = 0.7 (see Table 18-3). The level of uncertainty on the knowledge of ISR and FSR is of order 10%, reflecting the uncertainty on α_s. As a more conservative estimate of the resultant systematic errors in m_t, 20% of the Δm_t(ISR) and Δm_t(FSR) mass shifts defined above have been taken. The mass shifts and corresponding systematic errors are summarised in Table 18-3. The systematic errors estimated in this way are less than 0.3 GeV for ISR, while 1-2 GeV errors result from effects due to FSR.

An alternative approach uses the measured jet multiplicity to search, event-by-event, for the presence of hard gluon radiation. Following the convention for this approach adopted at the Tevatron [18-12], the mass shift would be defined not by comparing events with radiation switched on and events with radiation switched off, but by the difference, Δm_t, between the value of m_t determined from events with exactly four jets and that determined from events with

more than four jets. The systematic error due to effects of initial and final radiation would then be considered as $\delta m_t = \Delta m_t / \sqrt{12}$. Such a calculation would yield systematic errors of approximately 0.4 - 1.1 GeV, smaller than the more conservative approach adopted here.

Uncertainties in the size and shape of the background, which is dominated by 'wrong combinations' in $t\bar{t}$ events, can affect the top mass reconstruction. The resultant systematic uncertainty on m_t was estimated by varying the assumptions about the background shape in the fitting procedure. Fits of the m_{jjb} distribution were performed assuming a Gaussian shape for the signal and either a polynomial or a threshold function for the background. Varying the background function resulted in a systematic error on m_t of 0.2 GeV.

The structure of the 'underlying event' can affect the top mass reconstruction. However, as discussed in Section 18.1.3.4, it is possible to estimate and correct for this effect using data. Given the large statistics available at the LHC, it is assumed that the residual uncertainty from the underlying event will be small compared to the other errors (note that the 'underlying event' denotes here a minimum bias event, since the impact of ISR has already been accounted for).

The individual contributions to the systematic error of the inclusive and high p_T(top) samples are summarised in Table 18-3. For the inclusive sample, the systematic errors are reported for the analysis using jet cone sizes of ΔR = 0.4 and ΔR = 0.7. For the high p_T(top) sample, only ΔR = 0.4 was used since the jets are close in space.

Table 18-3 Top mass shift (Δm_t) and resulting systematic error on m_t (δm_t) due to the various source of systematic errors, for both the inclusive sample (for jet cone sizes of ΔR = 0.4 and 0.7) and the high p_T(top) sample. The light quark jet energy scale error for the high p_T(top) sample assumes that the W mass constraint cannot be used for an event-by-event calibration, due to the overlapping of the jets. See the text for more details.

Source of uncertainty	Comment on method	Inclusive sample		High p_T(top) sample	
		$\lvert\Delta m_t\rvert$ (GeV) ΔR=0.4 (0.7)	δm_t (GeV) ΔR=0.4 (0.7)	$\lvert\Delta m_t\rvert$ (GeV)	δm_t (GeV)
Light jet energy scale	1% scale error	0.3 (0.3)	0.3 (0.3)	1.3	1.3
b-jet energy scale	1% scale error	0.7 (0.7)	0.7 (0.7)	0.7	0.7
b-quark fragmentation	(ε_b=-0.006)-(ε_b=-0.0035)	0.3 (0.3)	0.3 (0.3)	0.5	0.5
Initial state radiation	ISR ON - ISR OFF	0.2 (1.3)	0.04 (0.3)	0.4	0.1
Final state radiation	FSR ON - FSR OFF	10.2 (6.1)	2.0 (1.2)	7.9	1.6
Background	-	0.2 (0.2)	0.2 (0.2)	< 0.2	< 0.2

In summary, the jet energy scale and FSR dominate the systematic errors. The jet corrections required are a function of the p_T of the jet (see Chapter 9), and are smaller for high p_T jets. For this reason, it is hoped that ongoing studies of the jet calibration might allow one to reduce this source of systematic error for the high p_T(top) sample with respect to the inclusive one. However, results are presented here, assuming a 1% scale uncertainty, independent of jet p_T. For the high p_T(top) sample, the light quark jet scale is also significant, if the constraint $m_{jj} = m_W$ cannot be used to calibrate the light quark jets event-by-event. The tightly collimated jets in the high p_T(top) sample require the use of a relatively small jet cone (ΔR = 0.4), resulting in a significant sensitivity to FSR effects.

18.1.3.4 High p_T single lepton plus jets analysis with a large calorimeter cluster

For the high p_T(top) sample, the large boost forces the jets from the hadronic top decay close to each other in the detector, where they overlap. While this causes some difficulties for the standard reconstruction, where m_t is reconstructed as the invariant mass of the *jjb* system (as presented above), it gives rise to the possibility to reconstruct the top mass by collecting all the energy deposited in the calorimeter in a large cone around the top quark direction. Such a technique has the potential to reduce the systematic errors, since it is less sensitive to the calibration of jets and to the intrinsic complexities of effects due to leakage outside the smaller cones, energy sharing between jets, etc. Some results from a preliminary investigation [18-16] of the potential of this technique are discussed below.

The event selection was performed as in Section 18.1.3.2, although the p_T cut on the isolated lepton and the E_T^{miss} cuts were lowered to 20 GeV, and the jets were required to have $p_T > 20$ GeV. A jet cone of $\Delta R = 0.4$ was used for the lepton hemisphere, where, apart from radiation effects, only the *b*-jet is expected. In the hemisphere opposite to the lepton, where the three jets from the hadronic top decay are expected, a smaller jet cone size of $\Delta R = 0.2$ was used.

For accepted events, the two highest p_T non-*b*-tagged jets were combined with the highest p_T *b*- jet candidate in the hemisphere opposite to the lepton to form candidates for the *jjb* hadronic top decay. The selected *jjb* combination was required to have $p_T > 150$ GeV and $|\eta| < 2.5$. With these selection criteria, about 13 000 events would be expected in the mass window from 145 to 200 GeV, with a purity of 90%, for an integrated luminosity of 10 fb^{-1}. The reconstructed invariant mass of the *jjb* combination is shown in Figure 18-11. The direction of the top quark was then determined from the jet momenta. Figure 18-12 shows the distance ΔR in pseudorapidity azimuthal angle space between the reconstructed top direction and the true direction at the parton level, demonstrating good agreement between the measured direction and the true direction.

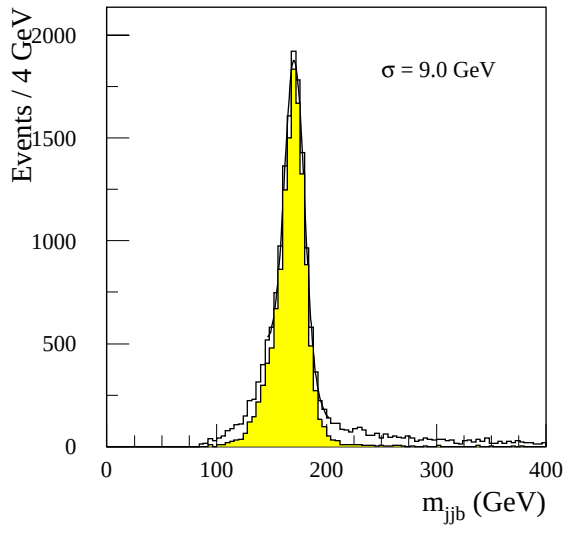

Figure 18-11 Invariant mass distribution of the selected *jjb* combination, using $\Delta R = 0.2$ cones for the high p_T (top) sample, normalised to an integrated luminosity of 10 fb^{-1}. The shaded area corresponds to the combinations with the correct jet-parton assignments.

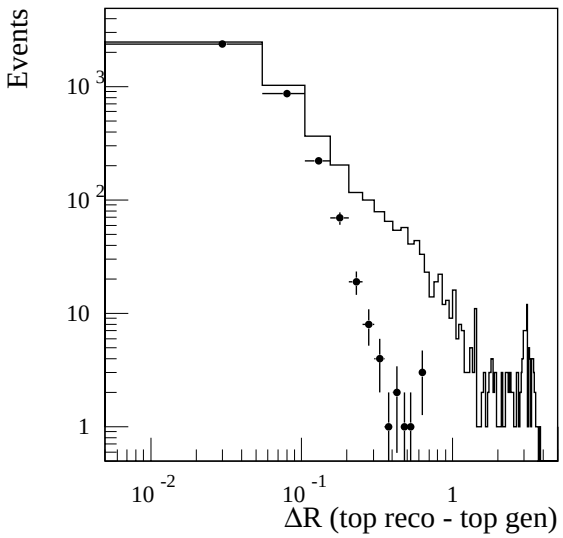

Figure 18-12 Distance ΔR between the top quark direction reconstructed using $\Delta R = 0.2$ cones and the parton level direction of the top quark. The dots correspond to the correct *jjb* combinations.

A large cone of radius ΔR was then drawn around the top quark direction as determined with jets of size 0.2. The top mass was determined by adding the energies of all calorimeter 'cells' within the cone (a calorimeter cell has a size $\Delta\eta x\Delta\phi$ = 0.1x0.1). The effective invariant mass of the cells was then calculated according to the formula:

$$m_{jjb} = (E^2 - p^2) = \left(\sum_{i=1}^{n} E_i\right)^2 - \left(\sum_{i=1}^{n} \vec{p}_i\right)^2 \quad ,$$

where the sum runs over all cells with energy above threshold inside the cone, the energies are those deposited in the cells, and the cell momenta are calculated from their energy and position, assuming the energy in each cell was deposited by a massless particle. The invariant mass spectrum is shown in Figure 18-13 for a cone size ΔR= 1.3, and exhibits a clean peak at the top quark mass.

The fitted value of the reconstructed top mass is shown in Figure 18-14, where it displays a strong dependence on the cone size. It has been checked that, if only the hard process (HP) in PYTHIA is enabled, the fitted mass remains constant (within 2%) independent of cone size. However, once effects of the 'underlying event' (UE) from multiple interactions (MUI) among the partons of the colliding pair of protons are included, a dependence on cone size appears. Additional shifts in the top mass result from initial and final state radiation (ISR / FSR).

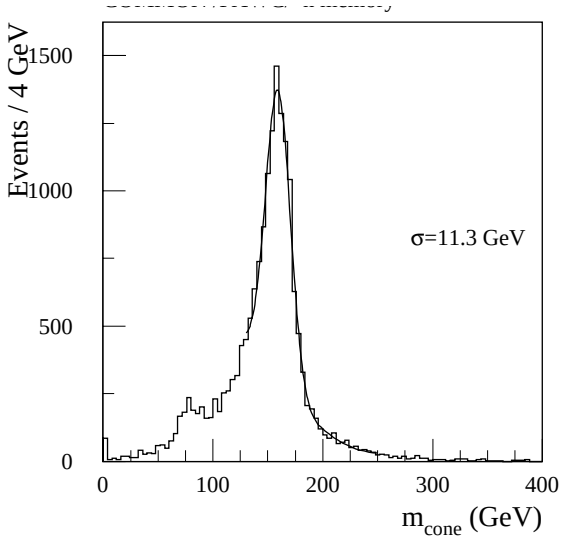

Figure 18-13 Reconstructed $t \rightarrow jjb$ mass spectrum obtained using cells in a single cone of size ΔR = 1.3, normalised to an integrated luminosity of 10 fb^{-1}.

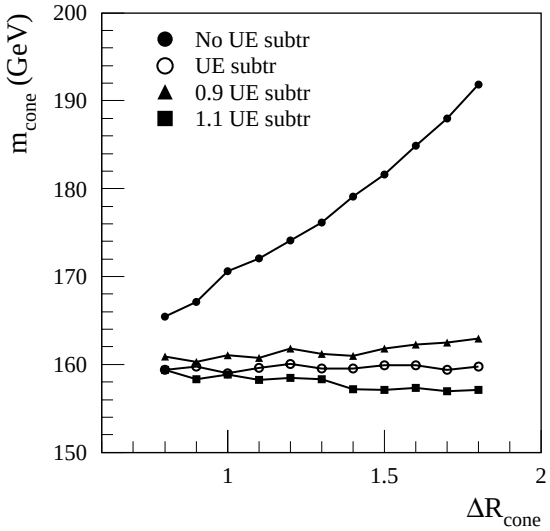

Figure 18-14 The fitted top mass using cells in a single cone, before and after the underlying event (UE) subtraction and as a function of the cone size.

In the absence of the underlying event, and for cone sizes which are sufficiently large to contain all three jets from the hadronic top decay, the fitted mass should be independent of the cone size. Therefore, a method has been developed to subtract the contribution from the underlying event, by using the calorimeter cells not associated with the products of the top quark decay. The UE contribution was calculated as the average E_T deposited per calorimeter cell, averaged over those cells which were at least a distance ΔR away from the impact points of the daughters of the partons in the hard scattering process. In Figure 18-15, the values obtained for different settings of the PYTHIA generator are shown. As expected, the average E_T per calorimeter cell

increases as more activity is added, especially in the case of ISR. Only a rather small dependence is observed on the radius ΔR used to isolate the cells associated with the hard scattering process.

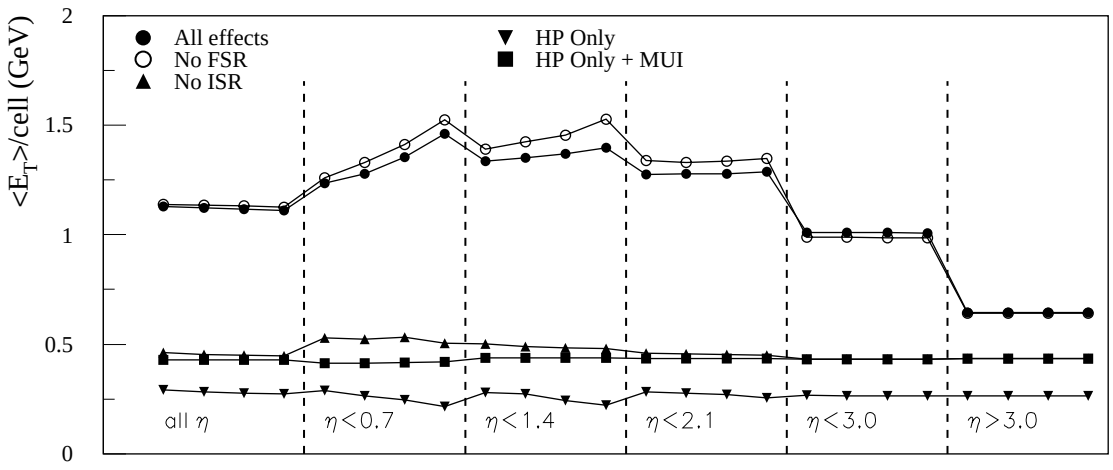

Figure 18-15 Estimator of the average E_T deposited per cell from the underlying event as a function of η for different settings of the PYTHIA event generator. In each η range, the four symbols correspond to different ΔR values, within which cells were flagged as belonging to partons from the hard scattering process (ΔR = 0.7, 0.8, 0.9, and 1.0) and therefore not used to compute the average E_T per cell. The acronyms of HP (hard-scattering process), MUI (multiple interactions), ISR (initial state radiation) and FSR (final state radiation) refer to the options enabled in PYTHIA for the various data sets.

For the remainder of the analysis, the average E_T per cell in the case of HP+MUI only (0.429 GeV per cell) was used as the UE estimator and was subtracted from each cell (assuming no pseudorapidity dependence) used in the invariant mass calculation. The resulting value of the reconstructed mass (m_{cone}), with and without UE subtraction, is shown in Figure 18-14 as a function of the cone radius. As can be seen, after the UE subtraction, the reconstructed top mass is independent of the cone size used. As a cross-check, the mean E_T per cell was varied by ±10% and the top mass recalculated in each case. As shown superimposed on Figure 18-14, these 'miscalibrations' lead to a re-emergence of a dependence of m_t on the cone size. While the prescription for the UE subtraction does lead to a top mass which is independent of the cone size, it should be noted that the reconstructed mass is about 15 GeV (or 8.6%) below the nominal value, m_t = 175 GeV, implying that a rather large correction would be needed.

To investigate if this correction can be calibrated, the same procedure was applied to a sample of W+jet events generated with a range of p_T comparable to that of the top sample. The W was forced to decay hadronically into jets. Events were selected by requiring the presence of at least 3 jets (using a cone size of 0.4) with $p_T > 30$ GeV and $|\eta| < 2.5$. The highest p_T jet was required to satisfy $p_T > 40$ GeV. The W decay was reconstructed from the second and third highest p_T jets, since in general the highest p_T jet was the jet balancing the p_T of the W boson.

As for the high p_T(top) analysis, the direction of the reconstructed W was measured from the jets, and all cells within a distance ΔR were used to calculate the W invariant mass. The underlying event contribution was estimated with the same algorithm as described above, averaging over those cells which were far away from the reconstructed jets. The results agreed within 1% with the values determined for the high p_T(top) sample. This is not surprising since the underlying event contribution measured without ISR is expected to be basically identical for all processes.

In Figure 18-16, the reconstructed W mass as a function of the cone size is plotted before and after the UE event subtraction. As in the case of the top events, the reconstructed W mass after UE subtraction is independent of the cone size. The average value of m_{jj} after the UE subtraction is about 8.5 GeV (or 10.6%) below the nominal value of m_W.

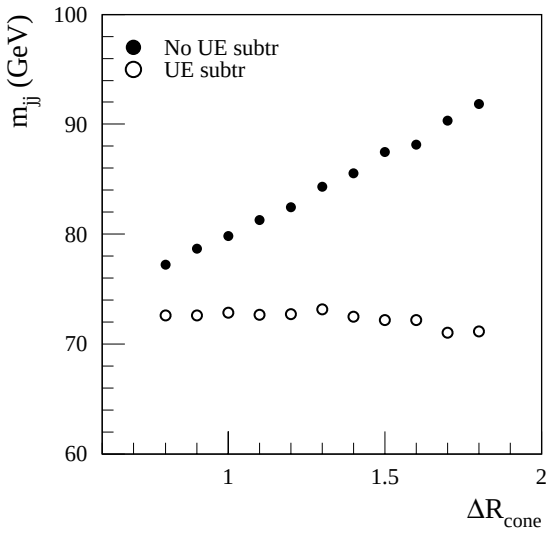

Figure 18-16 For the W+jet sample, the fitted W mass, using cells in a single cone, before and after the UE event subtraction and as a function of the cone size.

The fractional error on m_{jj}, as measured with the W+jet sample, was used as a correction factor to m_{cone} in the high p_T(top) sample. For a cone of radius ΔR = 1.2, the top mass after UE subtraction increases from 160.1 GeV to 177.0 GeV after rescaling. Similarly, the value of 159.9 GeV, obtained after UE subtraction with a cone of radius ΔR = 1.3, gives a value of 176.0 GeV after rescaling. The rescaled values of m_{cone} are about 1% higher than the generated top mass. This over-correction of m_t using the value of m_W measured with the same method, is due to ISR contributions to the cone used to measure m_t. If ISR is switched off, the rescaling procedure works to better than 1%. This can be understood, since the contributions from ISR to high p_T $W \rightarrow jj$ decays, whether produced directly or in top decay, should be similar to first order in energy, but not in mass.

The systematic errors were evaluated as described in Section 18.1.3.3 and are summarised in Table 18-4. Varying the energy scale of the calorimeter cell calibration by 1% resulted in an error in m_t of 0.6 GeV. As expected, the use of a large cone substantially reduces the effects of FSR and b-quark fragmentation, each of which gives rise to a systematic error of 0.1 GeV. The uncertainty arising from ISR, which can affect the determination of the UE subtraction, is about 0.1 GeV. The main uncertainty in this technique comes from the calibration procedure. The calibration with the W+jet sample produces a value of m_t which is about 1% above the generated value. Furthermore, the $W \rightarrow jj$ events would suffer from background from QCD multi-jet events. Ongoing studies suggest one could calibrate using $W \rightarrow jj$ decays from the high p_T(top) events themselves, selecting those events in which the b-tagged jet is far away from the other two jets of the W decay and then reconstructing the $W \rightarrow jj$ decay using a single cone of size ΔR = 0.8. For example, requiring that the minimum separation between the light quark jets and the b-tagged jets satisfy $\Delta R > 1.5$, one can see a clear W mass peak, as shown in Figure 18-17. Further study is required to reliably estimate the potential of this calibration procedure, and a systematic uncertainty of 1% is assigned to it in Table 18-4.

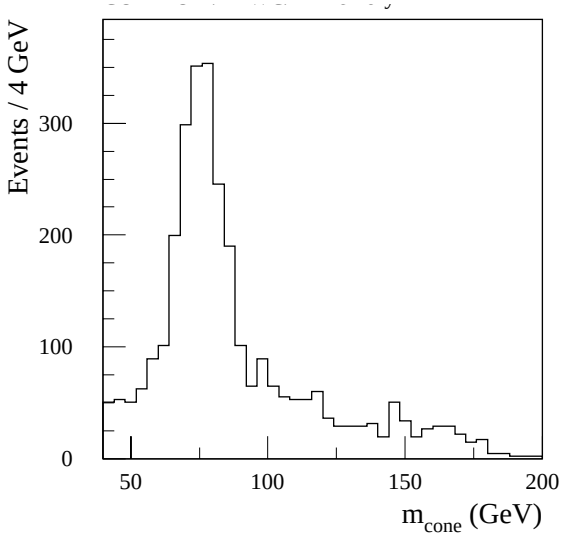

Figure 18-17 Reconstructed $W \rightarrow jj$ mass spectrum obtained using cells in a single cone of size ΔR = 0.8, for those events of the high p_T(top) sample where the b-tagged jets are a distance of at least ΔR = 1.5 away from the light quark jets. The figure is normalised to an integrated luminosity of 10 fb^{-1}.

Table 18-4 Top mass shift (Δm_t) and resulting systematic error on m_t (δm_t) due to the various sources of systematic errors (see text), for the high p_T(top) sample analysed using cells in a large cone ΔR = 1.3.

Source of uncertainty	Comment on method	Cone size ΔR = 1.3	
		$\lvert\Delta m_t\rvert$ (GeV)	δm_t (GeV)
Cell energy scale	1% scale error	0.6	0.6
b-quark fragm.	(ε_b=-0.006)-(ε_b=-0.0035)	0.1	0.1
Initial state radiation	ISR ON - ISR OFF	0.7	0.1
Final state radiation	FSR ON - FSR OFF	0.2	0.1
Calibration of method	High p_T $W \rightarrow jj$ decays	1.6	1.6

18.1.3.5 Comparison between fast and full simulation for the single lepton plus jets sample

The computing power required to generate sufficiently large $t\bar{t}$ samples to perform all the systematic studies would be prohibitive. However, in order to be able to cross-check the results obtained with ATLFAST, a total of over 60 000 $t\bar{t}$ events were processed through DICE, the GEANT-based ATLAS detector simulation, and then the ATLAS reconstruction package, ATRECON. The event samples included approximately 30 000 inclusive single lepton plus jet events, and an equal number of events generated with p_T(top) > 200 GeV.

To avoid simulating events through GEANT which would later likely fail the selection criteria, cuts on the transverse momentum and pseudorapidity of the $t\bar{t}$ daughters have been applied at the generator level. The fully simulated events have, therefore, been generated under somewhat more restrictive conditions than used for the ATLFAST simulations described previosuly. In order to make consistent comparisons between fast and full simulation, the events which have been passed through the full GEANT simulation and reconstruction package were also run through the fast simulation package (ATLFAST), so that the exact same events can be compared (see also Section 9.3.4).

For the inclusive channel, in the top mass window 175 ± 35 GeV, the signal purity and overall efficiency were P = 79% and ε = 6.4% for fast simulation and P = 78% and ε = 5.7% for full simulation. Figure 18-18 and Figure 18-19 show the m_{jj} mass distributions for the two reconstructions. The resulting m_W resolutions were 7.3 and 8.1 GeV for fast and full simulation, respectively. The reconstructed m_{jjb} invariant mass distributions are shown in Figure 18-20 and Figure 18-21. The m_{jjb} invariant mass resolutions were 11.4 GeV and 13.4 GeV for fast and full simulation, respectively .

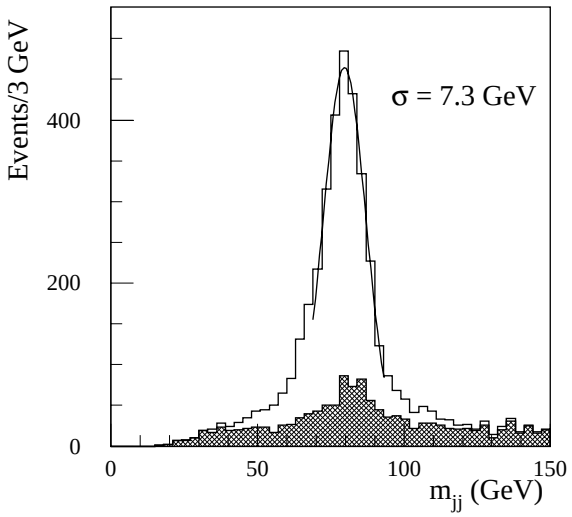

Figure 18-18 Invariant di-jet mass distribution obtained from fast simulation for the same sample of 30 000 inclusive single lepton plus jet events which were fully simulated. The shaded histogram shows the background from wrong combinations.

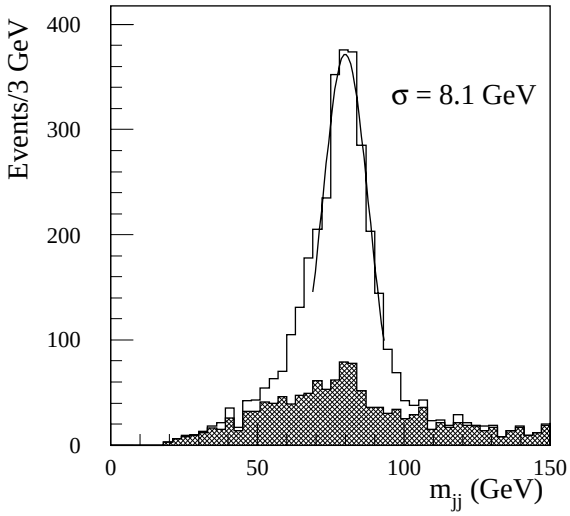

Figure 18-19 Invariant di-jet mass distribution obtained from full simulation for the sample of 30 000 inclusive single lepton plus jet events. The shaded histogram shows the background from wrong combinations.

In summary, the predictions from the two simulations are in good agreement for the signal efficiencies and purities. The amount and shape of the combinatorial background under the W and top mass peak are in good agreement as well. The m_W and m_t mass resolutions are in reasonable agreement, with the full simulation predicting resolutions which are 10-20% worse than those from the fast simulation.

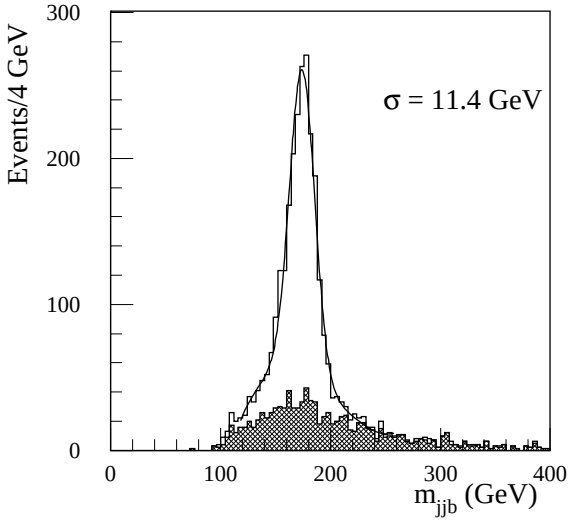

Figure 18-20 Invariant *jjb* mass distribution obtained from fast simulation for the same sample of 30 000 inclusive single lepton plus jet events which were fully simulated. The shaded histogram shows the background from wrong combinations.

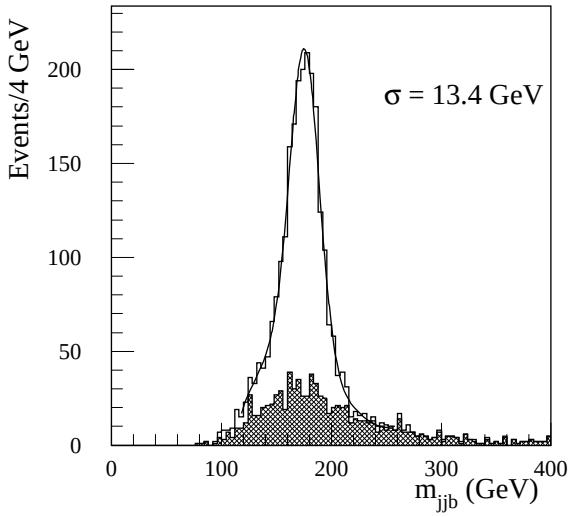

Figure 18-21 Invariant *jjb* mass distribution obtained from full simulation for the sample of 30 000 inclusive single lepton plus jet events. The shaded histogram shows the background from wrong combinations.

18.1.3.6 Dilepton channel

Dilepton events can provide a measurement of the top quark mass complementary to that obtained from the single lepton plus jets mode. The signature of a dilepton event consists of two isolated high p_T leptons, high E_T^{miss} due to the neutrinos, and two jets from the fragmentation of the *b*-quarks. Measurement of m_t using dilepton events is complicated by the fact that one cannot fully reconstruct either of the top quarks, due to the undetected neutrinos in the final state. This problem can be dealt with by weighting each solution based on some dynamical information, and thus obtaining a preferred mass for each event. Alternatively, one can take advantage of the fact that the kinematical distributions of the top decay products depend on m_t, and attempt to obtain the most likely top mass for a set of events. The mass determination depends on the assumption that the kinematical distributions for top production are reproduced by the Monte Carlo simulation.

About 400 000 dilepton $t\bar{t}$ events are expected to be produced in a data sample corresponding to an integrated luminosity of 10 fb^{-1}. Backgrounds arise from Drell-Yan processes associated with jets, $Z \rightarrow \tau\tau$ associated with jets, WW+jets and $b\bar{b}$ production. The event selection criteria required two opposite-sign leptons within $|\eta| < 2.5$, with $p_T > 35$ and 25 GeV respectively, and with $E_T^{miss} > 40$ GeV. Two jets with $p_T > 25$ GeV were required in addition. After the selection cuts, 80 000 signal events survived, with *S/B* around 10.

Of the many possible kinematic variables which could be studied, preliminary analyses [18-17] of three have been performed: the mass m_{lb} of the lepton-*b*-jet system, the energy of the two highest E_T jets, and the mass m_{ll} of the dilepton system formed with both leptons coming from the same top decay (*i.e.* $t \rightarrow lvb$ followed by $b \rightarrow lvc$).

Top mass measurement using m_{lb}

In this analysis, the value of m_t was estimated using the expression

$$m_t^2 = m_W^2 + 2 \cdot \langle m^2_{lb} \rangle / [1 - \langle \cos\theta_{lb} \rangle]$$

Here, $<m_{lb}^2>$ is the squared mean invariant mass of the lepton and *b*-jet from the same top decay. The mean value of $\cos\theta_{lb}$, the angle between the lepton and the *b*-jet in the *W* rest frame, can be regarded as an input parameter to be taken from Monte Carlo.

To obtain a very clean sample, the two highest p_T jets were required to be tagged as *b*-jets, leaving a total of about 15,200 signal events per 10 fb^{-1}. One cannot determine, in general, which lepton should be paired with which *b*-jet. The pairing which gave the smaller value of m_{lb}^2 was chosen, and checking the parton-level information showed that this criterion selected the correct pairing in 85% of the cases, for a generated top mass of 175 GeV. The mean value $<m_{lb}^2>$ was measured for samples generated with different top masses *m*, and then m_t was calculated from the expression above. The resultant m_t is a function of $<\cos\theta_{lb}>$ and *m*. A χ^2 was defined and minimised with respect to $<\cos\theta_{lb}>$ in order to determine the best value of $<\cos\theta_{lb}>$. The value of m_t was corrected to compensate for the shift, less than 0.6 GeV, produced by using a fixed $<\cos\theta_{lb}>$, and for not distinguishing between *b* and $\bar{b}$.

For an integrated luminosity of 10 fb^{-1}, the expected statistical uncertainty on m_t using this method is about 0.9GeV. Major sources of systematics include uncertainty on the *b*-quark fragmentation function, which produces a systematic error on m_t of 0.7 GeV if defined as described in Section 18.1.3.3. Systematic errors due to the effects of FSR and ISR together are about 1 GeV, while that due to varying the jet energy scale by 1% is 0.6 GeV. Further studies are required to estimate the uncertainties due to the reliance upon the Monte Carlo modelling of the $t\bar{t}$ kinematics.

Top mass measurement using energy of two leading jets

Increased sensitivity could be obtained with a technique which utilizes not only the mean, but also the shape of the kinematic distribution. As an example, a study has been made of the sensitivity to m_t obtained by comparing to 'template' distributions the energy of the two highest E_T jets. The template distributions were made by generating PYTHIA samples of $t\bar{t}$ events with different values of m_t in the range 160-190 GeV, in steps of 5 GeV. Figure 18-22 shows, as an example, the templates obtained for m_t = 165 GeV and 175 GeV.

For each possible top mass value m, a $\chi^2(m)$ was obtained by comparing the kinematical distribution of the simulated data with the templates of mass m. The best value for the mass was the value which, for the 'data' set, generated with m_t = 175 GeV, gave the minimum χ^2.

For an integrated luminosity of 10 fb^{-1}, the expected statistical sensitivity on m_t corresponds to about 0.4 GeV. Varying the calorimeter jet energy scale by 1% produced a systematic error on m_t of 1.5 GeV. Other sources of systematic error result from dependence of the method on the Monte Carlo modelling of the $t\bar{t}$ kinematics, and require further study. As an example, changing the choice of the structure functions used in the Monte Carlo simulation (for example, from CTEQ2L to CTEQ2M or EHQL1) led to differences in the top mass of ±0.7 GeV.

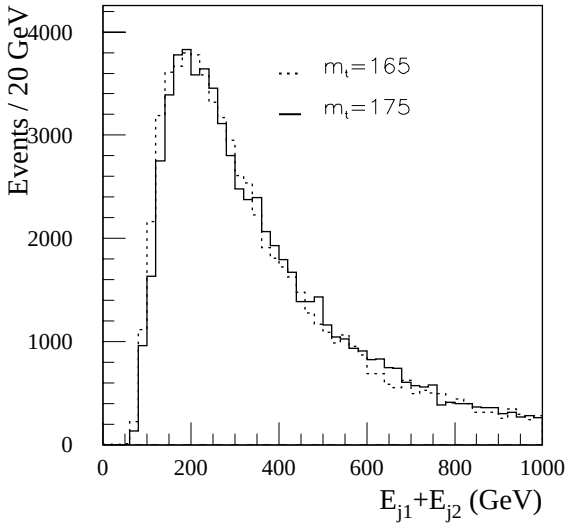

Figure 18-22 Template distributions of the total energy of the two leading jets in $t\bar{t}$ events for top quark masses of 165 and 175 GeV. The two distributions are normalised to the same area.

Top mass measurement using m_{ll} in tri-lepton events

The invariant mass distribution of the two leptons from the same top quark decay (*i.e.* $t \to lvb$ followed by $b \to lvc$) is quite sensitive to m_t. It has been shown that the mass distribution of lepton pairs from the same top quark decay is much less sensitive to the top quark transverse momentum distribution than that of lepton pairs from different top quarks [18-18].

Signal events are expected to contain two leptons from the decay of the W bosons produced directly in the top and anti-top quark decays, and one lepton from the b-quark decay. In addition to the cuts described above, one non-isolated muon with $p_T > 15$ GeV was required.

For an integrated luminosity of 10 fb^{-1}, the expected signal would be about 7,250 events, yielding a statistical uncertainty on the measurement of m_t of approximately ±1 GeV. This technique is insensitive to the jet energy scale. The dominant uncertainties arise from effects of ISR and FSR and from the b-quark fragmentation, which sum up to about 1.5 GeV.

18.1.3.7 Summary of top mass studies

The very large samples of top quark events which will be accumulated at the LHC will allow a precision measurement of the top quark mass. More than 120 000 single lepton plus jet events would be selected, with a signal-to-background ratio of over 60, within a single year of running at low luminosity. Measuring m_t by reconstructing the invariant mass of the $t \to jjb$ candidates in these events would yield a statistical error below 0.1 GeV. Studies of the systematic errors indicate a total error below 2 GeV should be obtainable, provided the energy scales for jets and b-jets can be understood at the 1% level (see Chapter 12). A substantial contribution to the systematic error for the inclusive sample comes from FSR. A method to reconstruct m_t in the high p_T(top) sample using the cells within a single large cone, succeeds in substantially reducing the

sensitivity to FSR. Further study is required to reliably estimate the potential of this method. Complementary measurements of m_t can be performed with the sample of 80 000 dilepton events selected for an integrated luminosity of 10 fb^{-1}.

18.1.4 Top quark pair production

The NLO prediction for $t\bar{t}$ production at the LHC is quite precisely known. At the LHC, the gluon-gluon fusion process $gg \rightarrow t\bar{t}$ accounts for about 90% of the total $t\bar{t}$ production, with $q\bar{q}' \rightarrow t\bar{t}$ accounting for the rest. (Note that these fractions are approximately reversed in the case of $p\bar{p} \rightarrow t\bar{t}$ at the Tevatron, where $q\bar{q}'$ annihilation dominates). Measurements of the total cross-section, as well as differential cross-sections, are discussed in Section 15.8.4, including implications for QCD measurements, such as the determination of parton distribution functions. Here some examples of possible signatures of new physics in $t\bar{t}$ production are presented.

18.1.4.1 $t\bar{t}$ production cross-section measurements

Physics beyond the SM could affect cross-section measurements for $t\bar{t}$ production in a variety of ways. For example, existence of a heavy resonance decaying to $t\bar{t}$ might enhance the cross-section, and might produce a peak in the $t\bar{t}$ invariant mass spectrum (this possibility is discussed in more detail in the next section). Deviations from the SM top quark branching ratios, due for example to a large rate of $t \rightarrow H^+b$, could lead to an apparent deficit in the $t\bar{t}$ cross-section measured with the assumption that BR($t \rightarrow W^+b$) ≈ 1.

The NLO prediction of $\sigma(t\bar{t})$ = 833 pb [18-1] implies production of over 8 million $t\bar{t}$ pairs in one year at low luminosity. Measurements of $\sigma(t\bar{t})$ will be limited by the uncertainty of the integrated luminosity determination, which is currently estimated to be 5%-10% (see Chapter 13). The cross-section relative to some other hard process, such as Z production, should be able to be measured more precisely.

18.1.4.2 Search for $t\bar{t}$ resonances

A number of theoretical models predict the existence of heavy resonances which decay to $t\bar{t}$. An example within the Standard Model is the SM Higgs boson, which will decay to $t\bar{t}$ provided the decay is kinematically allowed. However, the strong coupling of the SM Higgs boson to the W and Z implies that the branching ratio to $t\bar{t}$ is never very large. For example, for m_H = 500 GeV, the SM Higgs natural width would be 63 GeV, and BR($H \rightarrow t\bar{t}$) ≈ 17%. The resulting value of $\sigma \times$ BR for $H \rightarrow t\bar{t}$ in the SM is not sufficiently large to see a Higgs peak above the large background from continuum $t\bar{t}$ production. In the case of MSSM, however, if m_A,$m_H > 2m_t$, then BR($H/A \rightarrow t\bar{t}$) ≈ 100% for tan$\beta \approx 1$. For the case of scalar or pseudoscalar Higgs resonances, it has been pointed out [18-19] that interference can occur between the amplitude for the production of the resonance via $gg \rightarrow H/A \rightarrow t\bar{t}$ and the usual gluon fusion process $gg \rightarrow t\bar{t}$. The interference effects become stronger as the Higgs' mass and width increase. Searches for these decays are discussed in detail in Section 19.3.2.7, in the context of MSSM.

The possible existence of heavy resonances decaying to $t\bar{t}$ arises in technicolor models [18-20] as well as other models of strong electroweak symmetry breaking [18-21][18-22]. In Section 21.2.1.5, the production and decay into $t\bar{t}$ of a colour octet techni-eta (η_8) particle of mass 500 GeV was studied. Recent variants of technicolor theories, such as Topcolor [18-23], posit

new interactions which are specifically associated with the top quark, and could give rise to heavy particles decaying to $t\bar{t}$. Since $t\bar{t}$ production at the LHC is dominated by gg fusion, colour octet resonances ("colourons") could also be produced [18-24].

Because of the large variety of models and their parameters, a study was made of the sensitivity to a 'generic' narrow resonance decaying to $t\bar{t}$ (more details can be found in reference [18-25]). Events of the single lepton plus jets topology $t\bar{t} \rightarrow WWb\bar{b} \rightarrow (l\nu)(jj)b\bar{b}$ were selected by requiring $E_T^{miss} > 20$ GeV, and the presence of an isolated electron or muon with $p_T > 20$ GeV and $|\eta| < 2.5$. In addition, it was required that there were between four and ten jets, each with $p_T > 20$ GeV and $|\eta| < 3.2$. At least one of the jets was required to be tagged as a b-jet. After these cuts, the background to $t\bar{t}$ resonant production was dominated by continuum $t\bar{t}$ production.

The momentum of the neutrino was reconstructed, as described previously, by setting $m_\nu = 0$, assigning $E_T(\nu) = E_T^{miss}$, and calculating $p_z(\nu)$ (with a quadratic ambiguity) by applying the constraint that $m_{l\nu} = m_W$. The hadronic $W \rightarrow jj$ decay was reconstructed by selecting pairs of jets from among those not tagged as b-jets. In cases where there were at least two b-tagged jets, then candidates for $t \rightarrow Wb$ were formed by combining the $W \rightarrow l\nu$ and $W \rightarrow jj$ candidates with each of them. In events with only a single b-tagged jet, this was assigned as one of the b-quarks and each of the still unassigned jets then was considered as a candidate for the other b-quark.

Among the many different possible jet-parton assignments, the combination was chosen that minimised the following χ^2:

$$\chi^2 = (m_{jjb} - m_t)^2 / \sigma^2(m_{jjb}) + (m_{l\nu b} - m_t)^2 / \sigma^2(m_{l\nu b}) + (m_{jj} - m_W)^2 / \sigma^2(m_{jj})$$

Events were rejected if either $m_{l\nu b}$ or m_{jjb} disagreed with the known value of m_t by more than 30 GeV.

For events passing the reconstruction procedure, the measured energies were rescaled, according to their resolution, to give the correct values of m_W and m_t for the appropriate combinations. This procedure improved the resolution of the mass reconstruction of the $t\bar{t}$ pair to $\sigma[m_{t\bar{t}}] / m_{t\bar{t}} \approx 6.6\%$. As an example, Figure 18-23 shows the reconstructed $m_{t\bar{t}}$ distribution for a narrow resonance of mass 1600 GeV. The width of the Gaussian core is well described by the resolution function described above. The size of the tails, which are dominated by incorrect jet-parton assignments, is such that approximately 65% of the events are contained within $\pm 2\sigma$ of the peak.

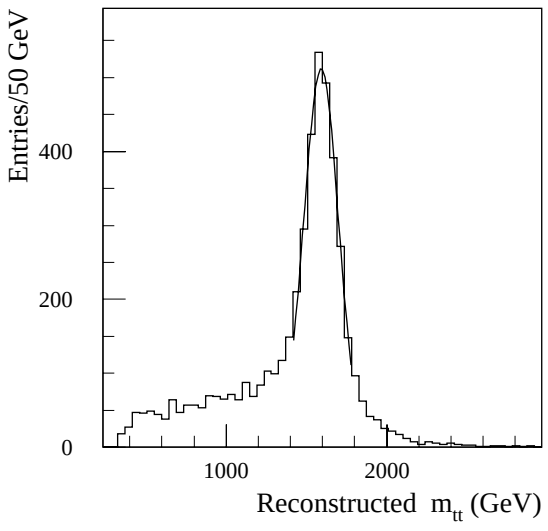

Figure 18-23 Measured $t\bar{t}$ invariant mass distribution for reconstruction of a narrow resonance of mass 1600 GeV decaying to $t\bar{t}$.

The reconstruction efficiency, not including branching ratios, for $t\bar{t} \rightarrow WWb\bar{b} \rightarrow (l\nu)(jj)b\bar{b}$ was about 20% for a resonance of mass 400 GeV, decreasing gradually to about 15% for $m_{t\bar{t}} = 2$ TeV.

For a narrow resonance X decaying to $t\bar{t}$, Figure 18-24 shows the required $\sigma \times \mathrm{BR}(X \rightarrow t\bar{t})$ for discovery of the resonance. The criterion used to define the discovery potential was observation within a $\pm 2\sigma$ mass window of a signal above the $t\bar{t}$ continuum background, where the required signal must have a statistical significance of at least 5σ and must contain at least ten events. Results are shown versus m_X for integrated luminosities of 30 fb^{-1} and 300 fb^{-1}. For example, with 30 fb^{-1}, a 500 GeV resonance could be discovered provided its $\sigma \times \mathrm{BR}$ is at least 2,560 fb. This value decreases to 830 fb for m_X = 1 TeV, and to 160 fb for m_X = 2 TeV. The corresponding values for an integrated luminosity of 300 fb^{-1} are 835 fb, 265 fb, and 50 fb for resonances masses m_X = 500 GeV, 1 TeV, and 2 TeV.

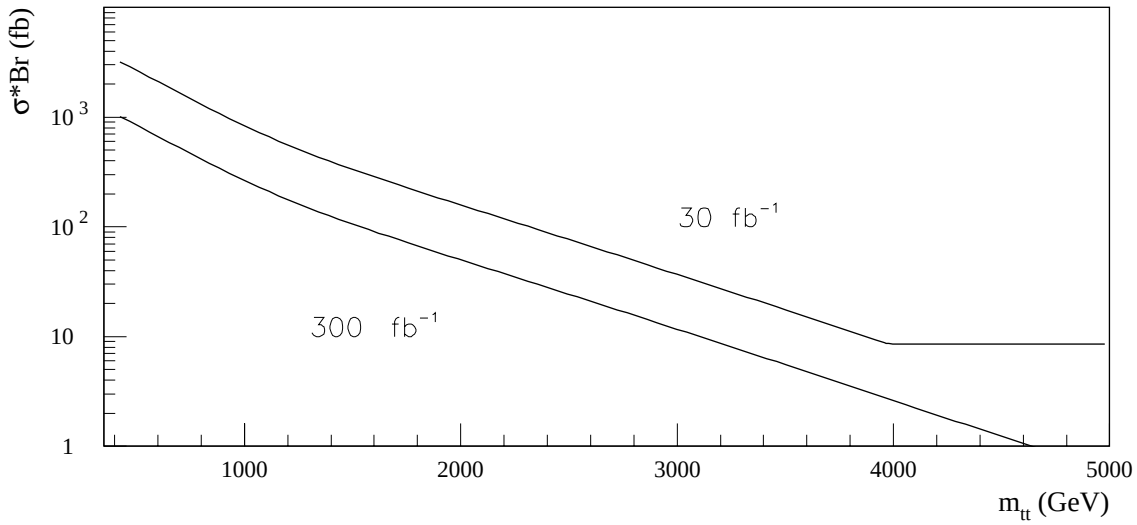

Figure 18-24 Value of $\sigma \times \mathrm{BR}$ required for a 5σ discovery potential for a narrow resonance decaying to $t\bar{t}$, as a function of $m_{t\bar{t}}$, and for an integrated luminosity of either 30 or 300 fb^{-1}.

Once predictions from models exist for the mass, natural width, and $\sigma \times \mathrm{BR}$ for a specific resonance, the results in Figure 18-24 can be used to determine the sensitivity and discovery potential for those models. As discussed above, extra care must be taken in the case of spin zero resonances, due to possible interference effects. While such effects are small for the case of a narrow resonance, they can be significant once the finite widths of heavy resonances are taken into account.

18.1.4.3 $t\bar{t}$ spin correlations

The SM prediction of the top quark width, given the large value of m_t, is $\Gamma_t \sim 1.5$ GeV. Thus, the top quark lifetime is very short in comparison with the hadronisation time ($\sim 1/\Lambda_{\mathrm{qcd}}$), and the top quark decays as a "bare quark" before hadronising. In addition, the top quark decays before the strong interaction has time to depolarise its spin. As a consequence, the spin orientation of the top quark should be preserved in its decay. The weak decay of the top quark implies the daughters in the decay chain can be used to analyze its spin orientation.

To lowest order, top quarks produced via the strong processes $gg / q\bar{q} \rightarrow t\bar{t}$ are unpolarised, and the transverse polarisation effects due to loop diagrams are predicted to be very small. However, the spins of the t and $\bar{t}$ are correlated. At the LHC, the top and anti-top quarks tend to be produced with the same helicity, thus favouring the production of 'Left-Left' (LL) or 'Right-Right' (RR) $t\bar{t}$ pairs. For example, for $m_{t\bar{t}} < 500$ GeV, about 80% $t\bar{t}$ pairs are predicted [18-26] to be pro-

duced with either LL or RR helicities. This fraction falls slowly to a little under 70% for $m_{t\bar{t}} < 1000$ GeV. A measurement of this spin correlation would check whether the top quark does indeed decay before the strong interaction has time to depolarise its spin, and thereby would allow a lower limit to be set on Γ_t. Furthermore, new physics, such as large CP violation in the top system, could alter the spin correlations predicted by the SM. Such effects could result, for example, from additional phases in the EWSB sector which, due to the large value of m_t, could produce large effects in top physics while still satisfying bounds from data on the lighter quarks (see, for example, [18-27]).

The angular distribution of the ith decay product with respect to the top spin vector is given, in the top quark rest frame, by the expression:

$$\frac{1}{N}\frac{dN}{d\cos\theta_i} = \frac{1}{2}(1 + \alpha_i \cos\theta_i)$$

The coefficients α_i are characteristic for each particle produced in the decay ($\alpha = 1$ for charged leptons, $\bar{d}$ and $\bar{s}$ quarks; $\alpha = -0.33$ for neutrinos, u and c quarks; $\alpha = -0.41$ for the b-quark). From these values, it is apparent that the charged lepton, in addition to being the simplest to tag experimentally, also provides the most undiluted measure of the top spin direction. Therefore, the analysis presented here will consider only the correlations between the pair of charged leptons produced in 'dilepton' $t\bar{t}$ events where both W bosons decay via $W \rightarrow l\nu$.

For dilepton $t\bar{t}$ events, the angular distribution of the two charged leptons is described by:

$$\frac{1}{N}\frac{d^2N}{d(\cos\theta_{l_1})d(\cos\theta_{l_2})} = \frac{1}{4}(1 - \kappa \cos\theta_{l_1}\cos\theta_{l_2})$$

with $\kappa = A\alpha_{l1}\alpha_{l2}$, where $A = (2P\text{-}1)$ and P is the fraction of the events where the top and anti-top quarks are produced with the same helicity. As discussed above, $\alpha_{l1} = 1$ and $\alpha_{l2} = -1$.

For this analysis [18-28], Monte Carlo events have been generated with the default version of PYTHIA, which does not incorporate spin correlations, and also with a modified version where the matrix element for top decay takes into account the top polarisation:

$$|M|^2 \sim \frac{m_t^2 E_l (m_t - 2E_l)}{(q^2 - m_W^2)^2 + \Gamma^2 m_W^2}(1 + h_t \cos\theta_l)$$

where E_l and θ_l are the energy and the angle with respect to the top spin direction of the lepton, as measured in the top rest frame, and q is the lepton+neutrino 4-momentum. Predictions from the standard non-correlated PYTHIA matrix elements (NC) would correspond in this approach to the choice $(h_t, h_{\bar{t}}) = (0, 0)$. The SM prediction would correspond to $(h_t, h_{\bar{t}}) = (+1, -1)$. CP violation in top production and decay could give rise to different values for $(h_t, h_{\bar{t}})$. To investigate the effects of CP violation, the sets of values $(h_t, h_{\bar{t}}) = (0.2, -0.8)$ (referred to hereafter as 'CP28') and $(h_t, h_{\bar{t}}) = (0.9, -0.6)$ (dubbed 'CP96') were considered.

Physical observables, such as the opening angle between the two isolated leptons ($\cos\theta_{ll}$) and the azimuthal angle difference (ϕ_{ll}), are sensitive to h_t and were therefore chosen as good experimental probes of the $t\bar{t}$ spin correlations. As mentioned previously, the predicted spin correlations are a function of $m_{t\bar{t}}$. For dilepton events, $m_{t\bar{t}}$ cannot be directly measured due to the

missing neutrinos. However, a variety of possible kinematic variables, such as the dilepton invariant mass, are loosely correlated with $m_{t\bar{t}}$, and can be used as a crude estimator of $m_{t\bar{t}}$ to enhance the expected spin correlations.

Dilepton events were selected with the criteria described in Section 18.1.3.6. Two high p_T (larger than 35 and 25 GeV respectively) isolated, opposite-sign leptons with $|\eta| < 2.5$ and with $|m_{ll} - m_Z| > 10$ GeV were required, together with $E_T^{miss} > 40$ GeV and two jets with $p_T > 15$ GeV. In order to preserve statistics, *b*-tagging was not required. For each model, these criteria selected about one million dilepton events for an integrated luminosity of 100 fb^{-1}, with $S/B = 7.8$.

Figure 18-25(a) shows the measured $cos\ \theta_{ll}$ distribution in the case of the various parameter sets. The bin-by-bin fractional differences between the measured distributions for the SM and those for the other models considered are shown in Figure 18-25(b) for the case of no correlations (NC), in Figure 18-25(c) for CP28, and in Figure 18-25(d) for CP96. The same distributions for the azimuthal angle difference ϕ_{ll} are shown in Figure 18-26. The solid line shows the case where all events are considered, while the dashed (dotted) lines shows the result for those events with $m_{ll} < m_Z$ ($m_{ll} > m_Z$) .

For both angles, differences at the level of a few percent are observable between the distributions measured for the different models. The differences for the CP96 model are somewhat less pronounced than for CP28, as expected given the smaller deviation of the spin parameters from the SM values. Further study is required to more fully explore the sensitivity to CP violation.

18.1.5 Top quark decays and couplings

Within the context of the Standard Model, the top quark decays as a 'bare quark' via a pure V-A interaction. The decay $t \to W^+b$ is dominant according to the SM, with a branching ratio of approximately 99.9%. Expectations for the CKM-suppressed decays are approximately 0.1% and 0.01% for $t \to W^+s$ and $t \to W^+d$, respectively. However, the large top mass implies that the top quark would tend to couple strongly to other massive particles. Therefore, determining whether the top quark has the couplings and decays predicted by the SM provides a sensitive probe of physics beyond the SM.

18.1.5.1 BR($t \to bX$) and measurement of V_{tb}

The SM prediction that BR($t \to W^+b$) ≈ 1 can be checked by comparing the number of $t\bar{t}$ events with a double *b*-tag to those with a single *b*-tag. In this manner, the first *b*-tag is used to identify the event as a $t\bar{t}$ event, and the presence of a second *b*-tag is then used to determine the fraction of top quark decays involving a *b*-quark, and hence a measurement of BR($t \to bX$). Within the three-generation SM,

$$R_{2b/1b} = BR(t \to Wb) / BR(t \to Wq) = |V_{tb}|^2 / (|V_{tb}|^2 + |V_{ts}|^2 + |V_{td}|^2) = |V_{tb}|^2.$$

Therefore, within the context of the SM, with unitarity of the three-generation CKM matrix, $R_{2b/1b}$ provides a measure of $|V_{tb}|$. Applying the unitarity constraint, the value of $|V_{tb}|$ is already very precisely known; the Particle Data Group [18-29] lists the allowed range of values from 0.9991 to 0.9994. However, new physics, such as the existence of a fourth generation of quarks, would imply the three-generation CKM matrix is not unitary, and could increase the relative branching ratios of $t \to W^+s(d)$ compared to $t \to W^+b$.

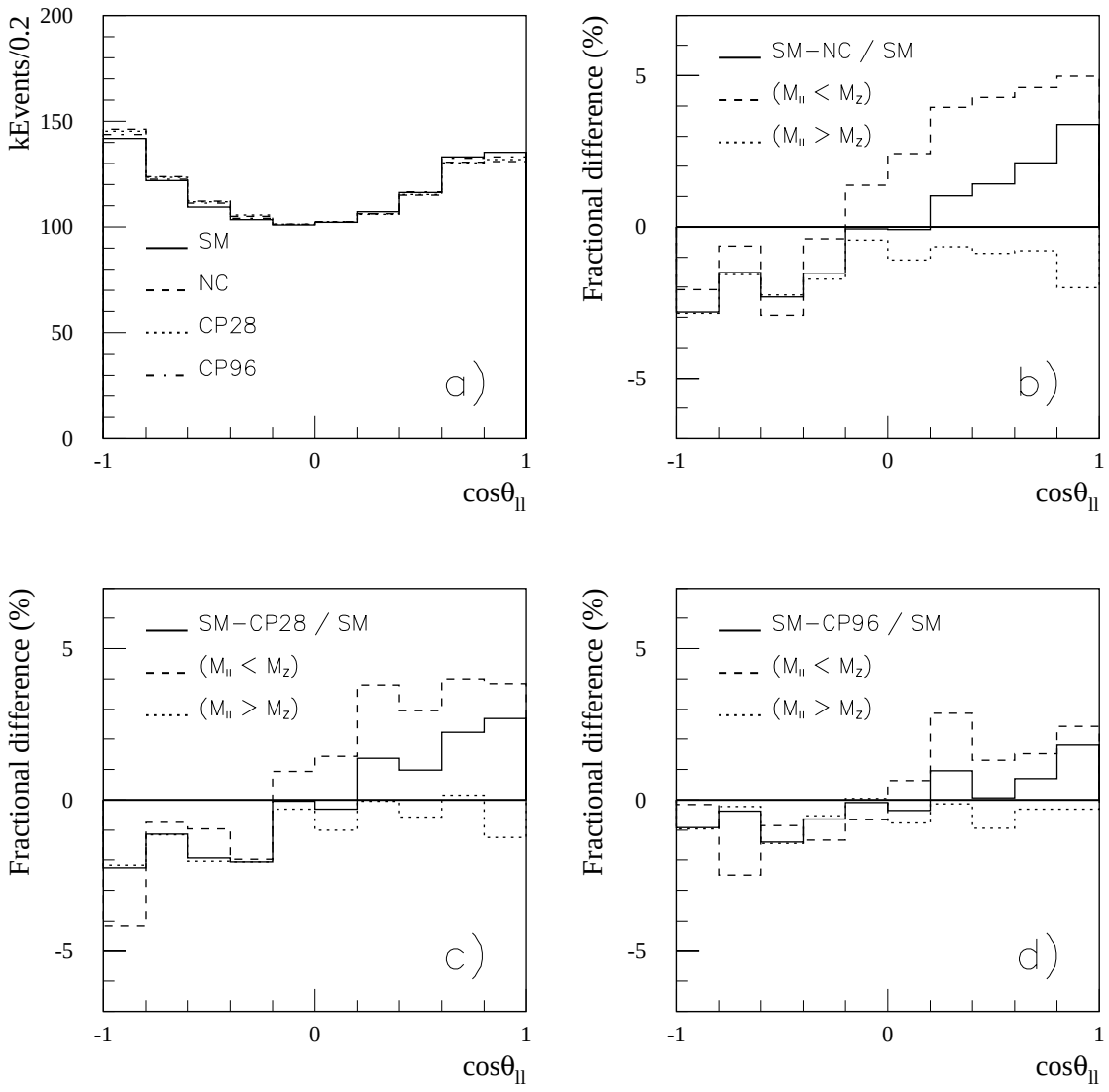

Figure 18-25 (a) Distribution of $cos\,\theta_{ll}$ as measured for the various parameter sets, normalised to 100 fb^{-1}. Also, fractional differences between the SM distribution and that measured with (b) no spin correlations (NC), (c) the CP28 parameter set, and (d) the CP96 parameter set. In each plot, the solid line shows the distribution for all events, and the dashed (dotted) line shows the results for events with $m_{ll} < m_Z$ ($m_{ll} > m_Z$). For more details, see the text.

CDF has measured the ratio of double *b*-tags to single *b*-tag in leptonic $t\bar{t}$ events, and determined a value of $R_{2b/1b} = 0.99 \pm 0.29$ [18-30], consistent with the SM expectation within the large (predominantly statistical) error. Within the SM, this measurement implies $|V_{tb}| > 0.76$ (95% C.L.). Without the SM three-generation unitarity constraint, the measurement implies only that $|V_{tb}|$ is much larger than either $|V_{ts}|$ or $|V_{td}|$.

The very large samples of $t\bar{t}$ events which will be accumulated at the LHC will allow a statistically sensitive measurement of $R_{2b/1b}$. For example, as discussed earlier, $t\bar{t}$ events in the single lepton plus jets mode can be selected by requiring an isolated electron or muon with $p_T > 20$ GeV, $E_T^{miss} > 20$ GeV, and at least four jets with $p_T > 20$ GeV. Requiring that at least one of the jets be tagged as a *b*-jet produces a clean sample of $t\bar{t}$ events, with *S/B* = 18.6, with the re-

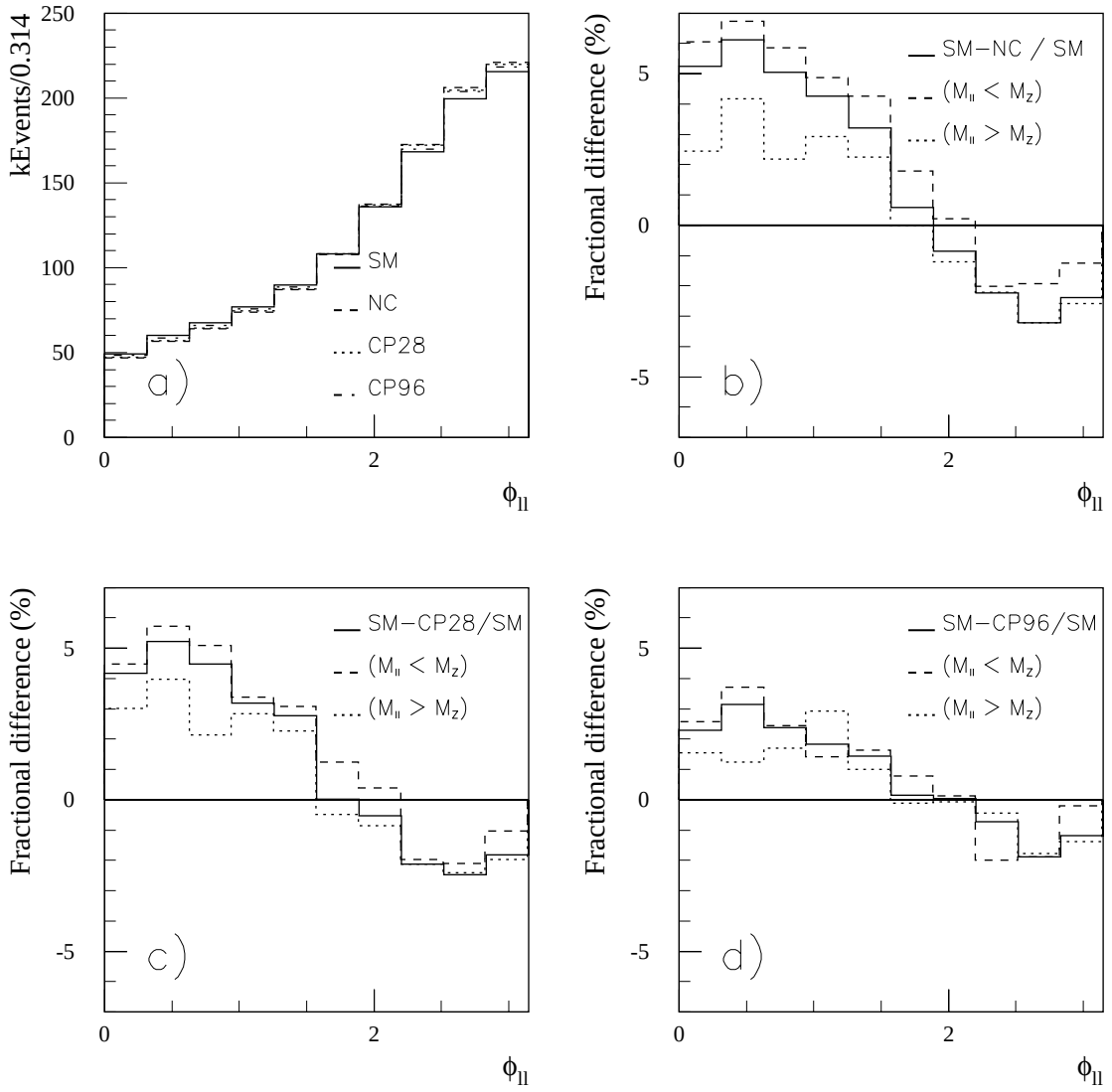

Figure 18-26 (a) Distribution of ϕ_{ll} as measured for the various parameter sets, normalised to 100 fb^{-1}. Also, fractional differences between the SM distribution and that measured with (b) no spin correlations (NC), (c) the CP28 parameter set, and (d) the CP96 parameter set. In each plot, the solid line shows the distribution for all events, and the dashed (dotted) line shows the results for events with $m_{ll} < m_Z$ ($m_{ll} > m_Z$). For more details, see the text.

maining background coming mostly from W+jet events. Assuming a b-tagging efficiency of 60%, a sample of 820 000 single b-tagged events would be selected for an integrated luminosity of 10 fb^{-1}. Of these, 276 000 would be expected to have a second b-tag, assuming the SM top quark branching ratios. Given these numbers, the statistical precision achievable would correspond to a relative error of $\delta R_{2b/1b} / R_{2b/1b}(\text{stat.}) \approx 0.2\%$ for an integrated luminosity of 10 fb^{-1}. The final uncertainty will be dominated by systematics errors due to the uncertainty in the b-tagging efficiency and fake b-tag rates, as well as correlations affecting the efficiency for b-tagging two different jets in the same event. Further study is needed to estimate the size of these systematic uncertainties.

18.1.5.2 BR($t \to WX$)

The measurement of the ratio ($R_{ll/l}$) of dilepton to single lepton $t\bar{t}$ events can be used to determine BR$(t \to WX)$. In this case, the first lepton tags the $t\bar{t}$ event, and the presence of a second lepton is used to determine the fraction of top quark decays producing an isolated lepton, which can be then be related to the presence of a W (or other leptonically decaying state) in the decay. The SM, for which BR($t \to WX$) = 100%, predicts $R_{ll/l}$ = BR($W \to l\nu$) ≈ 2/9. Deviations from this prediction could be caused by new physics. For example, the existence of a charged Higgs boson could lead to a large branching ratio for the decay $t \to H^+b$ if kinematically permitted. The dominant H^+ decays, in such instances, are usually considered to be $H^+ \to \tau\nu$ or $H^+ \to c\bar{s}$. In either of these cases, the number of isolated electrons and muons produced in top decay would be reduced, and so $R_{ll/l}$ would be less than the SM prediction. The existence of such a charged Higgs boson could also be probed by explicitly searching for an excess of τ production (see Section 18.1.5.4). However, it is possible the first sign of new physics could come from the more 'inclusive' measurement of $R_{ll/l}$.

As discussed above, with an integrated luminosity of 10 fb^{-1}, a clean sample of about 443 000 $t\bar{t}$ events in the single lepton plus jets mode could be selected by requiring an isolated electron or muon with p_T > 20 GeV, E_T^{miss} > 20 GeV, and at least two b-tagged jets with p_T > 20 GeV. To determine $R_{ll/l}$, one then measures how many of these events have a second isolated electron or muon, again with p_T > 20 GeV, and of the opposite sign of the first lepton. For an integrated luminosity of 10 fb^{-1}, and assuming the SM, one would expect a selected sample of about 46 000 dilepton events with these cuts. Given these numbers, the statistical precision achievable would correspond to a relative error of $\delta R_{ll/l} / R_{ll/l}$(stat.) ≈ 0.5% for an integrated luminosity of 10 fb^{-1}. Further study is required to estimate the systematic uncertainties in $R_{ll/l}$ due to the lepton identification and fake rates.

18.1.5.3 Top quark Yukawa coupling

In the SM, the mass of the top quark is due to its Yukawa coupling (y_t) to the Higgs boson. The values of the Yukawa couplings of the fundamental fermions are free parameters of the Standard Model. The measured value of m_t implies a value of the top quark Yukawa coupling of approximately unity. Alternative theories, such as Topcolor [18-23], explain the large top mass as arising, at least in part, from some new strong dynamics. Clearly, measuring independently the value of the Yukawa coupling would provide important information on the mechanism of fermion mass generation.

The value of the top quark Yukawa coupling can be accessed experimentally by searching for $t\bar{t}H$ production. One of the lowest order Feynman diagrams for this process of Higgs production in association with $t\bar{t}$ is shown in Figure 18-27. The top Yukawa coupling appears at the top-Higgs vertex. The reconstruction of this process is discussed in detail in Section 19.2.4.3 as part of the search strategy for both SM and MSSM Higgs bosons. Here the final results of the analysis are used to determine the precision implied for the determination of the top quark Yukawa coupling.

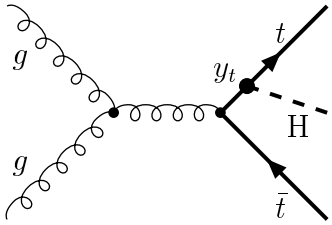

Figure 18-27 A lowest order Feynman diagram for $t\bar{t}H$ production.

The $t\bar{t}H$ analysis required one of the top quarks to decay via $t \to lvb$ and the other via $t \to jjb$. Since $t\bar{t}H$ production has a significant cross-section only for relatively light Higgs masses, the Higgs boson is detected through its decay $H \to b\bar{b}$, the dominant decay channel for the m_H range of interest. Thus, the final state contains an isolated lepton, missing p_T, two light quark jets, and a total of four b-jets. The resulting large combinatorial background was dealt with by first reconstructing both top quark decays. The combination which simultaneously best satisfied both the t and $\bar{t}$ mass constraints was used to assign jets to the top decays. A search was then made for a $H \to b\bar{b}$ signal using only the remaining unassigned b-jets.

Table 18-5 For an integrated luminosity of 30 fb^{-1}, and for three different values of m_H, the expected number of events for the signal from SM $t\bar{t}H$ production followed by the $H \to b\bar{b}$ decay. The final row provides the relative statistical uncertainty on the top quark Yukawa coupling.

	SM Higgs mass		
Process	**80 GeV**	**100 GeV**	**120 GeV**
$t\bar{t}H$ Signal	81	61	40
Total Backgnd	145	150	127
$\delta y_t/y_t$ (stat.)	9.3%	11.9%	16.2%

The expected numbers of signal and background events are summarised in Table 18-5 for SM Higgs masses of 80, 100, and 120 GeV, and for integrated luminosity of 30 fb^{-1}. The background events are mostly from $t\bar{t}$ production with additional jets. Results are given in Table 18-6 for 100 fb^{-1}.

Table 18-6 The same as Table 18-5, but for an integrated luminosity of 100 fb^{-1}.

	SM Higgs mass		
Process	**80 GeV**	**100 GeV**	**120 GeV**
$t\bar{t}H$ Signal	140	107	62
Total Backgnd	295	278	257
$\delta y_t/y_t$ (stat.)	7.4%	9.2%	14.4%

The implied statistical uncertainty in the determination of y_t is given in the last row in each table. For example, for m_H = 100 GeV, y_t could be measured with a relative statistical error of 11.9% for 30 fb^{-1}, improving to 9.2% for an integrated luminosity of 100 fb^{-1}. Many of the systematic errors, such as those associated with uncertainties in the integrated luminosity and in the $t\bar{t}$ reconstruction efficiency, could be controlled by comparing the $t\bar{t}H$ rate with the $t\bar{t}$ rate.

18.1.5.4 Top quark rare decays

With its large mass, the top quark will couple strongly to the sector of EWSB. Many models of physics beyond the SM include a more complicated EWSB sector, with implications for top quark decays. Examples include the possible existence of charged Higgs bosons, or possibly large flavor changing neutral currents (FCNC) in top decays. The sensitivity to some of these scenarios is discussed below.

$t \to H^+b$

If a sufficiently light charged Higgs boson exists, the decay $t \to H^+b$ could compete with the SM decay mode $t \to W^+b$. As discussed in Section 18.1.5.2, such a possibility could be seen by looking 'inclusively' at the ratio of dilepton to single lepton $t\bar{t}$ events. However, one could also look directly for evidence of this decay, for example by searching for a violation of lepton universality, whereby one finds an excess of τ production in $t\bar{t}$ events due to the decay $t \to H^+b$, followed by $H^+ \to \tau\nu$. The details of such an analysis for $t \to H^+b$ are presented in Section 19.3.2.11 in the context of exploring the Higgs sector of MSSM. As discussed in detail there, the limit on the sensitivity

to BR($t \to H^+b$) is dominated by systematic uncertainties, arising mainly from imperfect knowledge of the τ-lepton efficiency and of the number of fake τ-leptons present in the final sample. These uncertainties are estimated to limit the achievable sensitivity to BR($t \to H^+b$) = 3%.

Flavor Changing Neutral Currents (FCNC)

Within the SM, FCNC decays of the top quark are highly suppressed, and so any observation of FCNC top decays at the LHC would be an indication of new physics. For example, Table 18-7 summarizes branching ratios for FCNC top quark decays as predicted in the SM [18-31] and in the MSSM [18-32].

Table 18-7 Approximate branching ratios predicted for FCNC top quark decays in the SM and in MSSM. In each case, *q* is used to denote *u* or *c* quarks.

FCNC Decay	BR in SM	BR in MSSM
$t \to Zq$	$\approx 10^{-12}$	$\approx 10^{-8}$
$t \to \gamma q$	$\approx 10^{-12}$	$\approx 10^{-8}$
$t \to gq$	$\approx 10^{-10}$	$\approx 10^{-6}$

While the MSSM does enhance the branching ratios, they would still be too small to be observable. However, other extensions of the SM, including models with new dynamical interactions of the top quark, with multiple Higgs doublets, and with new exotic fermions, can lead to very significant enhancements of FCNC top decays [18-33]. Typically, the models include anomalous couplings with a coupling strength to quarks proportional to $\sqrt{m_q}$. These models can then accommodate large effects in top quark decays, while still satisfying the existing stringent limits on FCNC decays of the light quarks. Some of these models allow branching ratios for FCNC top decays of 10^{-3} - 10^{-2}, or even higher. The existing limits from CDF [18-34] are BR($t \to Zq$) < 33% and BR($t \to \gamma q$) < 3.3%, each at 95% CL, limited by the statistics of Run I at the Tevatron. The FCNC couplings can be parametrised in terms of the strength of the anomalous coupling κ and a scale Λ which characterizes the cut-off scale of new physics. For example, with this formulation, the partial width for the FCNC decay $t \to gq$ can be written as $\Gamma(t \to gq) = 4/3\ \alpha_s\ m_t{}^3\ (\kappa_g{}^2/\Lambda^2)$, and similar expressions can be written for $\Gamma(t \to \gamma q)$ and $\Gamma(t \to Zq)$ (see [18-33] for more details).

$t \to Zq$ decay

The sensitivity to the FCNC decay $t \to Zq$ (with $q = u, c$) has been analysed [18-35] by searching for a signal in the channel $t\bar{t} \to (Wb)(Zq)$, with the boson being reconstructed via the leptonic decay $Z \to ll$. The selection cuts required a pair of isolated, opposite sign, same flavor leptons (electrons or muons), each with $p_T > 20$ GeV and $|\eta| < 2.5$ and with $|m_{ll} - m_Z| < 6$ GeV.

Due to the clean $Z \to ll$ signature, the dominant backgrounds are due to large cross-section processes with Z bosons in the final state, namely Z+jet and WZ production. These backgrounds, along with the signal process, were generated via PYTHIA 5.7 and simulated using ATLFAST. Cuts on the Zq final state are not sufficient to effectively reduce the large Z+jet background. Therefore, the analysis relied also on cuts based on the Wb decay of the other top quark in the event. Two different possible decay chains have been considered: the first ('leptonic mode') where the W decays leptonically $W \to l\nu$, and the second ('hadronic mode') with $W \to$ jj. The hadronic W decay signature has a much larger branching fraction, but suffers from larger backgrounds.

The search in the leptonic mode required, in addition to the leptons from the Z boson decay, an additional lepton with $p_T > 20$ GeV and $|\eta| < 2.5$, $E_T{}^{miss} > 30$ GeV, and at least two jets with $p_T > 50$ GeV and $|\eta| < 2.5$. In addition, exactly one of the high p_T jets was required to be tagged as a b-jet.

After these cuts, the invariant mass spectrum of each Zq combination was formed from the $Z \to ll$ candidates taken with each of the non b-tagged jets. The Zq invariant mass resolution was 10.1 GeV. Combinations were accepted if m_{Zq} agreed with the known top mass within ± 24 GeV. The signal efficiency, not including the branching ratios for $Z \to ll$ and $W \to l\nu$, is summarised in Table 18-9 as a function of the various cuts. Also shown are the number of accepted background events, assuming an integrated luminosity of 100 fb^{-1}. In this channel, a value of BR($t \to Zq$) as low as 1.1x10^{-4} could be discovered at the 5σ level with an integrated luminosity of 100 fb^{-1}.

Table 18-8 Signal efficiency for the analysis of $t\bar{t} \to (Wb)(Zq)$ with $W \to jj$ and $Z \to ll$. Also listed are the numbers of accepted background events, assuming an integrated luminosity of 100 fb^{-1}.

Description of Cut	$t \to Zq$ Effic.(%)	Bkgnd Events
2l, 4 jets	14.9	60394
m_Z cut	12.8	50973
m_W cut	5.4	14170
b-tag	2.5	1379
$t \to W^+b$ mass cut	0.6	90
m_{Zq} cut	0.4	2

The search in the hadronic mode required, in addition to the $Z \to ll$ candidate, at least four jets with $p_T > 50$ GeV and $|\eta| < 2.5$. One of the jets was required to be tagged as a b-jet. To further reduce the background, the decay $t \to jjb$ was first reconstructed. A pair of jets, from among those not tagged as a b-jet, was considered a W candidate if $|m_{jj} - m_W| < 16$ GeV. W candidates were then combined with the b-jet, and considered as a top candidate if $|m_{jjb} - m_t| < 8$ GeV. For those events with an accepted $t \to jjb$ candidate, the invariant mass of the Z candidate with the remaining unassigned high p_T jets was calculated to look for a signal from $t \to Zq$ decays. Combinations were accepted if m_{Zq} agreed with the known top mass within ±24 GeV.

The signal efficiency, not including the branching ratios for $Z \to ll$ and $W \to jj$, is summarised in Table 18-8 as a function of the various cuts. Also shown are the number of accepted background events, assuming an integrated luminosity of 100 fb^{-1}. The results in Table 18-8 demonstrate that, in this channel a BR as low as 2.3x10^{-4} could be discovered at the 5σ level.

Combining the results from the leptonic and hadronic modes, a branching ratio for $t \to Zq$ as low as 10^{-4} could be discovered at the 5σ level with an integrated luminosity of 100 fb^{-1}.

Table 18-9 Signal efficiency for the analysis of $t\bar{t} \to (Wb)(Zq)$ with $W \to l\nu$ and $Z \to ll$. Also listed are the numbers of accepted background events, assuming an integrated luminosity of 100 fb^{-1}.

Description of Cut	$t \to Zq$ Effic.(%)	Bkgnd Events		
		Z+j	*W+Z*	$t\bar{t}$
3 lep; p_T>20GeV	43.2	945	1778	1858
E_T^{miss} > 30GeV	32.7	80	1252	1600
2 j; p_T>50 GeV	19.7	31	225	596
m_Z cut	16.8	24	180	29
b-tag	8.2	10	14	10
m_{Zq} cut	6.1	0	2	5

t → γq decay

The sensitivity to the FCNC decay $t \to \gamma q$ (with q = u, c) was analysed [18-36] by searching for a peak above background in the $m_{\gamma j}$ spectrum in the region of m_t. The requirement of a high p_T isolated photon candidate in $t\bar{t} \to (Wb)(\gamma q)$ events is not sufficient to reduce the QCD multi-jet background to a manageable level. Therefore,

the $t \to Wb$ decay of the other top (anti-) quark in the event was reconstructed using the leptonic $W \to l\nu$ decay mode of the W boson decay. The final state sought was therefore $t\bar{t} \to (Wb)(\gamma q) \to (l\nu b)(\gamma q)$.

The event selection criteria required the presence of an isolated photon with $p_T > 40$ GeV and $|\eta| < 2.5$, an isolated electron or muon with $p_T > 20$ GeV and $|\eta| < 2.5$, and $E_T^{miss} > 20$ GeV. Exactly 2 jets with $p_T > 20$ GeV were required, in order to reduce $t\bar{t}$ background. At least one of the jets was required to be tagged as a b-jet, and to satisfy $p_T > 30$ GeV and $|\eta| < 2.5$.

The $t \to l\nu b$ candidate was first reconstructed. For the two possible solutions of the neutrino momentum (determined as described previously), the resultant W boson was combined with the b-tagged jet, and the combination accepted as a top quark candidate if $m_{l\nu b}$ agreed with m_t within ±20 GeV. For events with an accepted $t \to l\nu b$ candidate, the $t \to \gamma q$ decay was sought by combining the isolated photon with an additional hard jet with $p_T > 40$ GeV and $|\eta| < 2.5$.

The invariant mass of the γj system was required to agree with the known value of m_t within ±20 GeV. The $m_{\gamma j}$ resolution with the cuts described above was 7.7 GeV (see Figure 18-28), and the signal efficiency (not counting branching ratios) was 3.3%, including a b-tagging efficiency of 60%.

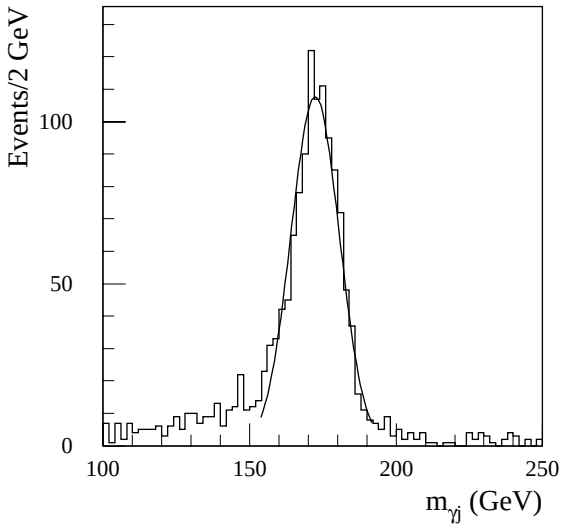

Figure 18-28 The $m_{\gamma j}$ invariant mass distribution resulting from the analysis of a sample of 10 000 signal events for the decay $t \to \gamma q$.

The background is dominated by events with a real $W \to l\nu$ decay and either a real or fake photon. These processes include $t\bar{t}$ and single top production as well as W+jets and $Wb\bar{b}$ production. The $t\bar{t}$ background was simulated with PYTHIA, while the other backgrounds were simulated as described in the discussion of the analysis of single top production presented in Section 18.1.6. After cuts, the background with real photons (normalised to an integrated luminosity of 100 fb^{-1}), consisted of 50 $t\bar{t}$ events, and negligible contributions from the other processes. Assuming a somewhat conservative jet rejection of about 2 900 for photons with $p_T > 40$ GeV (see Section 7.6), larger backgrounds resulted with fake photons, namely 90 $t\bar{t}$ events, 10 events from single top production, and about 5 events from W+jets including $Wb\bar{b}$. The total background was therefore 155 events, dominated by $t\bar{t}$ events. The corresponding 5σ discovery limit for an integrated luminosity of 100 fb^{-1} is BR($t \to \gamma q$) = 1.0×10^{-4}.

$t \to gq$ decay

A search for a FCNC t-gluon-q coupling (with $q = u,c$) through the decay $t \to gq$ would be overwhelmed by background from QCD multi-jet events. It has, however, been pointed out [18-37] that evidence for such a coupling can be sought through the production of like-sign top pairs, $pp \to ttX$ [$pp \to \bar{t}\bar{t}X$] (see Figure 18-29).

An experimentally clean signature of tt ($\bar{t}\bar{t}$) production would be the production of like-sign high p_T leptons, arising from events where the W bosons from both (anti-)top quarks decay leptonically. Such events would be expected to have, in addition to the like-sign lepton pair, two hard b-jets. The main sources of background are $qq \rightarrow Wq\mathrm{W}q$ and $qq' \rightarrow t\bar{t}\mathrm{W}$. The expected cross-section for each process producing W^+ pairs is about 0.5 pb, with that for W^- pairs about 0.25 pb.

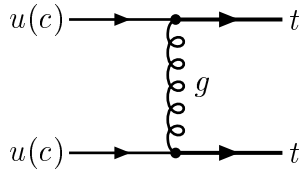

Figure 18-29 Feynman diagram depicting like-sign tt production via a FCNC t-gluon-q coupling (with $q = u, c$).

The initial selection required two like-sign isolated leptons with $p_T > 15$ GeV and $|\eta| < 2.5$. In addition, two jets with $p_T > 20$ GeV and $|\eta| < 2.5$ were required. Signal events should contain exactly two hard jets (due to the b-quarks), while the background events tend to contain additional jets. Thus, it was required that there exist no more than two jets with $p_T > 20$ GeV. These two leading jets were then required to have $p_T > 40$ GeV, and to have at least one tagged as a b-jet. In at least one of the two possible sets of lepton plus jet combinations, it was required that each of the lepton plus jet pairs have an invariant mass m_{lj} below 160 GeV, in order that they be kinematically consistent with originating from a top quark decay. Finally, it was required that the invariant mass of the $lljj$ system be greater than 500 GeV.

The effectiveness of the cuts in enhancing the signal relative to the background processes is summarised in Table 18-10. From initial samples of 10 000 events for each of the processes, 853 signal events survived all cuts, while only 15 $Wt\bar{t}$ and 12 $WqWq$ background events were retained. Scaling the backgrounds to their SM production cross-sections, a total of 10.8 $l^{\pm}l^{\pm}$ events (including all combinations of muons and electrons), would be expected for an integrated luminosity of 100 fb^{-1}. The results in Table 18-10 correspond to a 95% confidence level sensitivity to $|\kappa_g / \Lambda| = 0.091$ TeV^{-1}, corresponding to BR($t \rightarrow gq$) = 7.4 x 10^{-3}.

Table 18-10 Number of accepted same sign dilepton events for the same-sign top production signal and the $Wt\bar{t}$ and $WqWq$ backgrounds (out of an initial sample before cuts of 10 000 events in each case). The last line gives the equivalent number of accepted events assuming an integrated luminosity of 100 fb^{-1} and, in the case of the signal, for an anomalous coupling equal to unity.

Description of Cut	tt ($\bar{t}\bar{t}$) Signal	$Wt\bar{t}$ bkgnd	$WqWq$ bkgnd
Initial selection	3452	5354	5462
Exactly 2 jets	2095	712	3269
p_T(j) > 40 GeV	1221	316	118
$m_{lj} < 160$ GeV	1177	190	46
$m_{lljj} > 500$ GeV	853	15	12
Events / 100 fb^{-1}	22860	6.0	4.8

$t \rightarrow WbZ$ and $t \rightarrow WbH$

The 'radiative' top decay $t \rightarrow WbZ$ has been suggested [18-39] as a sensitive probe of the top quark mass, since the measured value of m_t is close to the threshold for this decay. For the top mass of (173 ± 5.2) GeV quoted by the 1998 Particle Data Group [18-29], the SM prediction is BR($t \rightarrow WbZ$) = (5.4$^{+4.7}_{-2.0}$) x 10^{-7} [18-39]. Thus, within the current uncertainty $\delta m_t \approx 5$ GeV, the predicted branching ratio varies by approximately a factor of three. A measurement of BR($t \rightarrow WbZ$) could, therefore, provide a strong constraint on the value of m_t. Similar arguments have been made for the decay $t \rightarrow WbH$, assuming a relatively light SM Higgs boson (*i.e.* for $m_H \approx m_Z$).

Sensitivity to the decay $t \to WbZ$ has been studied [18-36] using PYTHIA 6.1 and ATLFAST to simulate $t\bar{t} \to (WbZ)(Wb)$, with $Z \to ll$ and $W \to jj$. The efficiency for exclusively reconstructing $t \to WbZ$ is very low, due to the soft p_T spectrum of the b-jet in the $t \to WbZ$ decay. Instead, a 'semi-inclusive' technique was used, where a WZ pair close to threshold was searched for as evidence of the $t \to WbZ$ decay. Since the $t \to WbZ$ decay is so close to threshold, the resolution on m_{WZ} is not significantly degraded with respect to the exclusive measurement. The selection of $Z \to ll$ candidates required an opposite-sign, same-flavour lepton pair, each lepton having $p_T > 30$ GeV and $|\eta| < 2.5$. Since the $Z \to ll$ signal is so clean, a wide dilepton mass window was taken (60 GeV $< m_{ll} <$ 100 GeV) in order to have very high efficiency. Candidates for $W \to jj$ decay were formed by requiring at least two jets, each having $p_T > 30$ GeV and $|\eta| < 2.5$, and satisfying 70 GeV $< m_{jj} <$ 90 GeV. The $lljj$ invariant mass resolution was $\sigma[m_{WZ}] = 7.2 \pm 0.4$ GeV, and the signal efficiency was 4.3%.

The clean $Z \to ll$ signature means that the dominant backgrounds come from processes with a Z boson in the final state, primarily Z+jet production, and to a much lesser extent from WZ and $t\bar{t}$ production. In order to reduce the Z+jet background, an additional cut requiring a third lepton with $p_T > 30$ GeV was made. For the signal process $t\bar{t} \to (WbZ)(Wb)$, this cut selects events in which the W from the other top decays leptonically. The W leptonic branching ratio results in a corresponding drop in signal acceptance by a factor of about 2/9, but very effectively reduces the Z+jet background.

After the selection, and with a cut on m_{WZ} of ±10 GeV around the top mass, the total expected background was reduced to ≈1.5 events (mostly from WZ production) per 10 fb^{-1}. Requiring at least five events for signal observation leads to a branching ratio sensitivity of order 10^{-3}. Since the background has been reduced essentially to zero, the sensitivity should improve approximately linearly with integrated luminosity. However, even with a factor of ten improvement for an integrated luminosity of 100 fb^{-1}, the sensitivity would still lie far above the SM expectation of order 10^{-7}-10^{-6}.

Given this result, observation of the decay $t \to WbH$ does not look possible. The current LEP limit on m_H implies that the Higgs is sufficiently heavy that, in the most optimistic scenario that the Higgs mass is just above the current limit, BR(t $\to WbH$) ≈ BR(t $\to WbZ$). As m_H increases further, BR(t $\to WbH$) drops quickly. Assuming $m_H \approx m_Z$, one would have to search for $t \to WbH$ using the dominant decay $H \to b\bar{b}$. The final state suffers much more from background than in the case of $t \to WbZ$, where the clean $Z \to ll$ signature is a key element in suppressing background. Although BR($H \to b\bar{b}$) in this m_H range is much larger than BR($Z \to ll$), the large increase in background will more than compensate for the increased signal acceptance, and so one expects the sensitivity to BR($t \to WbH$) to be worse than for BR($t \to WbZ$). Therefore, the decay $t \to WbH$ has not been studied in further detail.

18.1.6 Electroweak single top quark production

As discussed above, the strong production of $t\bar{t}$ pairs yields large top quark samples, allowing detailed studies of many properties of top quark production and decay. However, the precise determination of the properties of the W-t-b vertex, and the associated coupling strengths, will more likely be obtained from measurements of the electroweak production of single top quarks. Single top quarks can be produced via three different reactions. These reactions are shown in Figure 18-30 from left to right in order of decreasing cross-sections.

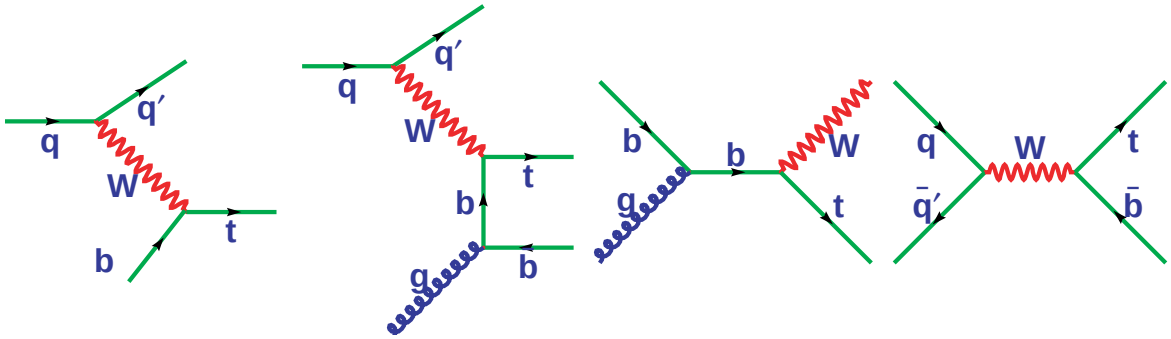

Figure 18-30 Feynman diagrams for the electroweak single top quark processes accessible at the LHC. The first two diagrams correspond to *W*-gluon fusion, the next to *Wt* production, and the final diagram to the *s*-channel or *W** process.

The first two graphs in Figure 18-30, usually referred to as the '2-2' and '2-3' processes, respectively, both refer to the same physical '*W*-gluon fusion' process. In this study the NLO correction as a separate process has been ignored. Rather, simulations based on the 2-2 process only have been used and normalised to the cross-section for a properly combined set of the two graphs. Since the *W*-gluon fusion process is the largest source of single top production at the LHC, with an expected cross-section of approximately 250 pb, it will be the source for much of the physics sensitivity, as well as a serious background for the other single top processes. The second production mechanism (the third graph from the left), referred to as the '*Wt*' process, is the direct production of a top quark and a *W* boson. This process is immeasurably small at the Tevatron, but is predicted to have a sizeable cross-section (≈60-110 pb) at the LHC. The third reaction proceeds via production of an off-shell *W* and will be called the '*W**' process. The cross-section for the *W** process is predicted to be only about 10 pb, since there are no valence anti-quarks in the initial state at the LHC.

Each process has a separate set of background sensitivities and experimental demands. Table 18-11 lists the cross-sections used in this study and the product of $\sigma \times BR$ for the case where one *W* decays leptonically via $W \to l\nu$, where the lepton is an electron or muon. This study is based upon an integrated luminosity of 30 fb^{-1}.

Table 18-11 Cross-sections used in the EW single top signal and background simulations.

Process	σ (pb)	$\sigma \times BR(W \to l\nu)$ (pb)
Wg (2-2 + 2-3)	244	54.2
Wt	60	17.8
W^*	10	2.2
$t\bar{t}$	833	246
$Wb\bar{b}$	300	66.7
Wjj	18000	4000

The primary physics interest in single top production is the ability to directly determine the coupling strength for the *t*-*W*-*b* vertex. The single top cross-section is unambiguously predicted by the SM (apart from the coupling), and it is important to cross check the *W*-gluon fusion, *Wt*, and *W** cross-sections separately. The various processes of single top production have different sensitivities to new physics. For example, the *W** channel is sensitive to an additional heavy *W'* boson, since new s-channel diagrams in which the W' is exchanged would occur. In contrast, additional contributions to the *W*-gluon fusion process from new t-channel diagrams with a *W'* would be suppressed by $1/m_{W'}{}^2$. Therefore, existence of a *W'* boson would be expected to produce an enhancement in both $\sigma(W^*)$ and $\sigma(W^*)/\sigma(Wg)$. On the other hand, the *W*-gluon fusion process channel is more sensitive to modifications of the top quark's couplings to the other SM particles. For example, an anomalous

chromo-magnetic moment in the top-gluon vertex [18-45], or a V+A contribution at the *t*-*W*-*b* vertex [18-46], could lead to both an increase in single top production and a modification of the decay angular distributions. Also, anomalous FCNC couplings could give rise to new contributions to single top production, such as $gu \rightarrow t$. These processes could modify the *W*-gluon process of single top production, while not affecting the rate of Wt and W^* channels. Therefore, in this case one would expect a decrease in the ratio of $\sigma(W^*)/\sigma(Wg)$.

Because it is an inherently weak production process, the *W* and top quark are produced in the appropriate mixture of helicities, as unambiguously predicted by the SM. A helicity analysis of top quark decay can check for new physics, such as right handed couplings, or an unexpected admixture of the left handed and longitudinal components for the *W*.

18.1.6.1 Monte Carlo generators

A variety of Monte Carlo generators have been employed to study electroweak single top production and the relevant backgrounds. The generators have been compared against one another for consistency and shown to be in reasonable agreement. All signal generators were interfaced to PYTHIA for showering and particle generation, with the PYTHIA output processed through ATLFAST for detector simulation. PYTHIA [18-5] includes the basic *W*-gluon fusion reaction according to SM assumptions. The SGPM package [18-47] is a parton-level generator for the Wt process, plus the $t\bar{t}$ and $Wb\bar{b}$ background processes. Also included are the FCNC processes, $gu \rightarrow t$ and $qq \rightarrow tt$. Decays are included and the reactions are implemented as external processes in PYTHIA. The ONETOP package [18-48] creates matrix elements at the parton level with the full density matrix for the 2-2, 2-3, W^* and Wt signal processes, as well as the $t\bar{t}$ and $Wb\bar{b}$ backgrounds. This is the only readily accessible generator which includes helicity information for all processes. Decays are included and all reactions are implemented as external processes in PYTHIA. HERWIG [18-6] has been used to produce *W*+jets background. Wjj events, involving the production of *W* in association with light quark jets, is a standard HERWIG process (iproc 2100). Background from $Wb\bar{b}$ is generated via a matrix element calculation interfaced to HERWIG.

Considerable effort was expended comparing the predictions of the various Monte Carlo generators. The results from PYTHIA, ONETOP, and SGPM for single top and $t\bar{t}$ production processes were very similar, agreeing typically within 10-15%. The predictions for the Wjj background were different by nearly 50%. The values from HERWIG are generally thought to be the most accurate, since HERWIG treats colour coherence more correctly, and were therefore used.

18.1.6.2 Signal and background separation strategies

In order to reduce the enormous QCD multi-jet backgrounds, as well as provide a high p_T lepton for trigger purposes, single top production with $t \rightarrow Wb$ followed by a leptonic decay $W \rightarrow l\nu$, where the charged lepton is a muon or an electron has been considered. The initial pre-selection cuts required the presence of at least one isolated lepton with $p_T > 20$ GeV, at least two jets with $p_T > 30$ GeV, and at least one *b*-tagged jet with $p_T > 50$ GeV. After these cuts, the dominant backgrounds are from processes with a real *W* in the final state, namely $t\bar{t}$ and Wjj (and in particular $Wb\bar{b}$) production. In the following, distributions are presented of variables which can be used to separate the various single top processes from these backgrounds and from each other.

Table 18-12 summarises the number of reconstructed jets per event, with $|\eta| < 5$ and $p_T > 15$ GeV, for the signal and background processes. It can be seen that the jet multiplicity would be a particularly useful variable for reducing the $t\bar{t}$ background, which has on average more jets than the single top processes.

Table 18-12 Fraction of events with different total reconstructed jet multiplicities for the various signal and background processes.

Process	njet = 2	njet = 3	njet > 3
W-g fusion	0.682	0.255	0.063
Wt	0.158	0.530	0.312
*W**	0.683	0.256	0.061
$t\bar{t}$	0.022	0.211	0.767
Wjj	0.446	0.323	0.231
W$b\bar{b}$	0.621	0.274	0.105

The number of jets per event tagged as *b*-jets, with $|\eta| < 2.5$, is presented in Table 18-13. It can be seen that requiring, for example, more than one *b*-tagged jet would enhance the *W** signal with respect to *Wjj* and *W*-gluon fusion. The reduction in the *W*-gluon fusion background is due to the fact that the second *b*-jet in *W*-gluon fusion events has low p_T and is often not tagged. In addition to the jet and *b*-jet multiplicities, the leading jet and *b*-jet p_T distributions are also useful discriminators. For example, the $Wb\bar{b}$ and *Wjj* events tend to have softer spectra than for single top and $t\bar{t}$ events.

Figure 18-31 shows the total event invariant mass, defined from the four vectors of all of the jets and leptons found in the event. A significant difference is observed between the invariant mass of events in the non-top backgrounds and in the signal processes.

This work focuses on single top signal events with a leptonic *W* decay. Therefore, apart from the *Wt* signal and the $t\bar{t}$ background, there should be no excess of di-jet combinations with m_{jj} near the value of m_W. Indeed, Figure 18-32 shows the distribution of di-jet masses obtained by choosing the di-jet with mass closest to m_W. It can be seen that *Wt* and $t\bar{t}$ have di-jet mass distributions which are significantly peaked near the *W* mass, while the other channels do not.

Table 18-13 Fraction of events with different total reconstructed *b*-jet multiplicities for the various signal and background processes.

Process	nb-jet = 1	nb-jet = 2	nb-jet > 2
W-g fusion	0.933	0.066	0.001
Wt	0.944	0.055	0.001
*W**	0.662	0.336	0.002
$t\bar{t}$	0.668	0.325	0.007
*W*jj	0.945	0.053	0.002
$Wb\bar{b}$	0.619	0.379	0.002

Another variable of interest is the reconstructed top mass (since there is no top quark in W*jj* and $Wb\bar{b}$ events). As described in previous sections, the top mass in the decay $t \to Wb$ followed by $W \to l\nu$ can be calculated by assigning $E_T(\nu) = E_T^{miss}$ and by calculating $p_z(\nu)$ (with a quadratic ambiguity) by applying the constraint that $m_{l\nu} = m_W$. Figure 18-33 shows the reconstructed $m_{l\nu b}$ distribution, where the $p_z(\nu)$ solution which gives $m_{l\nu b}$ closest to m_t has been chosen. In Figure 18-34, the scalar sum of the p_T of all of the jets in the event is plotted. Clearly the p_T in $t\bar{t}$ events is much higher on average than in the signal processes, while the *Wjj* events have lower average p_T .

Based on these kinematic distributions, cuts were optimised for each of the single top processes. In the case of *Wjj* production, the largest single top background, the cross-section at the LHC is currently not well known. Therefore, the usual procedure of minimising the relative error in the cross-section measurement by minimising $\sqrt{S+B}/S$ was not followed. Instead, the cuts were chosen to minimise the effect of the uncertainty on the W*jj* cross-section by optimising the *S/B*

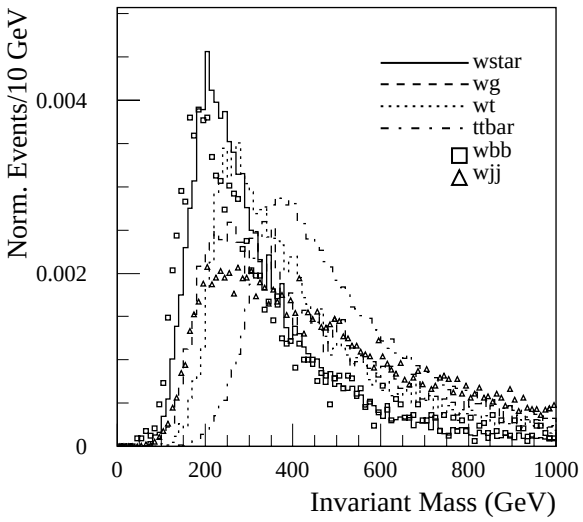

Figure 18-31 Total invariant mass of the event (see the text for more details), normalised to unity.

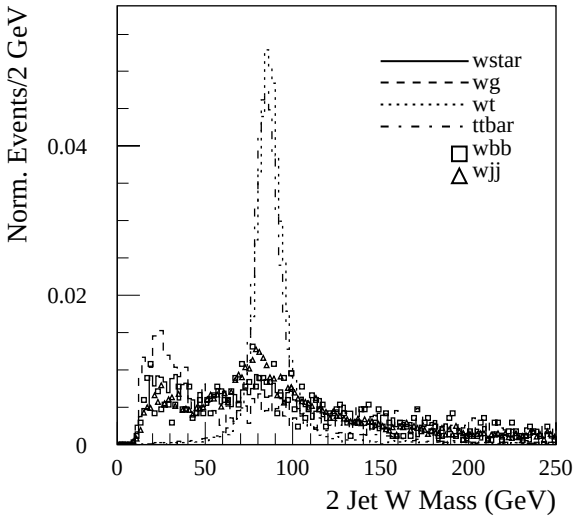

Figure 18-32 Invariant mass distribution of the di-jet with m_{jj} closest to m_W, normalised to unity.

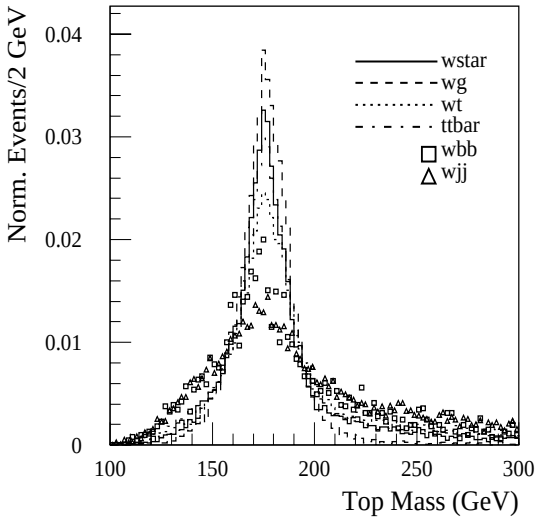

Figure 18-33 Invariant mass of the lνb combination with $m_{lνb}$ closest to m_t, normalised to unity.

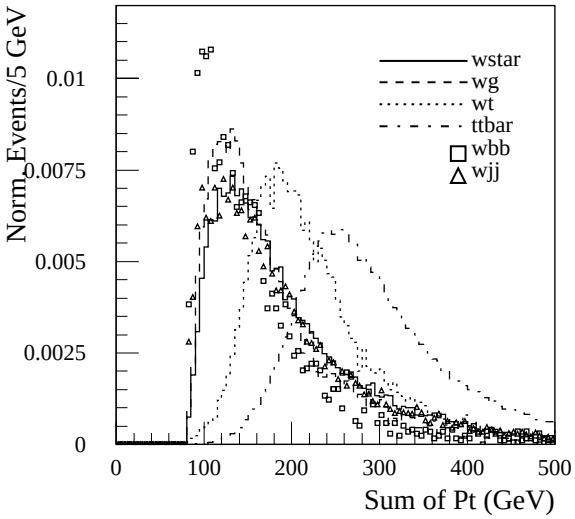

Figure 18-34 Scalar sum of p_T in each event, normalised to unity.

ratio. Analysis of each of the three single top production processes is presented in turn, followed in Section 18.1.6.6 by a discussion of the measurement of V_{tb}. The analysis of each process started with the pre-selection cuts presented earlier, namely the presence of at least one isolated lepton with $p_T > 20$ GeV, at least two jets with $p_T > 30$ GeV, and at least one *b*-tagged jet with $p_T > 50$ GeV.

18.1.6.3 Measurement of W-gluon fusion cross-section

The *W*-gluon signal is distinguished from backgrounds by the presence of a spectator quark jet which emerges in the forward direction. To isolate this signal, in addition to the pre-selection cuts, a forward jet with $|\eta| > 2.5$ and $p_T > 50$ GeV was therefore required. The total number of

jets was further required to be exactly two, to provide additional rejection of $t\bar{t}$ background, although it is recognised that comparison to a theoretical cross-section might be compromised by such a topological restriction. In addition, the central jet was required to be tagged as a *b*-jet, and to satisfy p_T > 50 GeV, in order to reduce *Wjj* background. Further rejection of the 'soft' *W*+jet backgrounds was accomplished by requiring the total invariant mass of the event be greater than 300 GeV and that H_T, the sum of the E_T values of all the jets and leptons in the event, satisfy H_T> 200 GeV. Finally, a top mass window was employed to reduce non-top backgrounds. These particular choices are not unique and a significant effort is still required to fully optimise these cuts. In particular, this will likely require a better understanding of the *Wjj* background.

Details of each cut are presented in Table 18-14 which shows the selection efficiency for the signal and background processes after each cut is applied, as well as the final number of events normalised to an integrated luminosity of 30 fb^{-1}. The number of events for the signal and $t\bar{t}$ background are taken as the average of results from ONETOP and PYTHIA. The number of events for the $Wb\bar{b}$ background are taken as the average of results from the HERWIG and ONETOP calculations. The result of 26 800 signal events and a total background of about 8 650 events, corresponds to a *S/B* = 3.1 and $S/\sqrt{B}$ = 286. The relative statistical uncertainty in the cross-section is 0.71%. If the high and low results of the *Wjj* calculation are used, the resulting values of S/B range from 4.3 down to 2.4.

Table 18-14 Cumulative efficiencies for the signal and background processes after each successive cut of the analysis to isolate the *W*-gluon fusion process. Also shown are the numbers of selected events after all cuts, normalised to an integrated luminosity of 30 fb^{-1}. The uncertainties are due to the Monte Carlo statistics. Note that the number of jets (Njets) includes any *b*-jets.

Description of cuts	Cumulative Selection Efficiency (%)			
	***W-g* fusion**	***tt***	**W*bb***	***Wjj***
Pre-selection cuts	20.0	44.4	2.49	0.667
Njets = 2; p_T>30GeV	13.2	0.95	0.99	0.37
Forward jet; p_T>50, $\|\eta\|$ >2.5	4.3	0.046	0.072	0.06
m_{tot}>300 GeV	3.58	0.025	0.043	0.048
H_T > 200 GeV	2.08	0.019	0.036	0.027
150 < m_t < 200 veto	1.64	0.01	0.0052	0.0066
Events / 30 fb^{-1}	26 800 ± 1000	720 ± 160	104 ± 60	7900 ± 1600

18.1.6.4 Measurement of *Wt* cross-section

The strategy for measuring the *Wt* cross-section is similar to that for *W*-gluon fusion, since they share the same backgrounds. However, the nature of *Wt* events makes them relatively easy to separate from *Wjj* and difficult to separate from $t\bar{t}$ events. Assuming the $t\bar{t}$ cross-section will be well measured at the LHC, this does not preclude performing a precise measurement of the *Wt* cross-section.

In addition to the pre-selection cuts, the number of jets in the central region was required to be exactly three, each with p_T > 50 GeV. Requiring at least three jets significantly reduces non-top backgrounds, while not allowing four or more jets reduces $t\bar{t}$ background. Exactly one of these jets was required to be tagged as a *b*-jet. By not allowing more than one *b*-tag the $t\bar{t}$ background

was reduced, while at least one *b*-tag was necessary to suppress *Wjj*. The total invariant mass of all reconstructed leptons and jets was required to be less than 300 GeV in a further attempt to reduce the $t\bar{t}$ background. Finally, the presence of a second *W* in *Wt* and $t\bar{t}$ events was exploited by requiring the reconstructed mass of the two untagged jets to be consistent with m_W by satisfying 65 GeV < m_{jj} < 95 GeV.

The samples of signal and background events surviving these cuts are summarised in Table 18-15. The only significant background remaining is from $t\bar{t}$ production, which is still more than a factor of four larger than the signal. Backgrounds from *Wjj* and from other single top processes are reduced to a negligible level. From Table 18-15, *S/B* = 0.22 and $S/\sqrt{B}$ = 39. The relative statistical error on the *Wt* cross-section is 2.8%.

Table 18-15 Cumulative efficiencies for the signal and background processes after each successive cut of the analysis to isolate the *Wt* process. Also shown are the numbers of selected events after all cuts, for an integrated luminosity of 30 fb^{-1}. The uncertainties listed are due to the Monte Carlo statistics. Note that the number of jets (Njets) includes any *b*-jets.

Description of cuts	Cumulative Selection Efficiency (%)		
	Wt	***tt̄***	***Wbb̄***
Pre-selection cuts	25.5	44.4	2.49
njets = 3; p_T > 50 GeV	3.41	4.40	0.05
n*b*-jet = 1	3.32	3.24	0.037
m_{tot} < 300 GeV	1.43	0.71	0.008
65 < m_{jj} < 95 GeV	1.27	0.41	0.003
Events / 30 fb^{-1}	6828 ± 269	30408 ± 742	58 ± 19

18.1.6.5 Measurement of *W** cross-section

Since the *W** signal has such a small cross-section relative to background, stringent cuts must be made to obtain a reasonable signal-to-background ratio (for details of this analysis see reference [18-49]). In addition to the pre-selection cuts, exactly two jets with $|\eta| < 2.5$ were required, in order to reduce the $t\bar{t}$ background, which tends to have more than two jets. Furthermore, both jets were required to have p_T > 75 GeV, and to be tagged as *b*-jets. This cut significantly reduces the *W*+jets background. This cut also reduces background from *W*-gluon fusion events since the second, lower p_T, *b*-jet from these events tends to be very soft and is often outside the *b*-tagging region ($|\eta|$<2.5). Those *W*-gluon fusion events for which both *b*-jets are tagged, are suppressed by the p_T cut. Further rejection of *Wjj* background is achieved by requiring the scalar sum of the jet p_T to be greater than 175 GeV, since the total jet p_T in *Wjj* events is generally lower than for events containing top quarks. The invariant mass of the event was required to exceed 200 GeV, again a cut predominantly against *Wjj* background events, which do not contain top quarks and so tend to have smaller invariant mass. Finally, a cut was placed on $m_{l\nu b}$, requiring it to lie within the range from 150-200 GeV.

The signal and background samples passing the successive cuts are summarised in Table 18-16. After all cuts, a value of S/B = 0.46 is achieved, with a significance of $S/\sqrt{B}$ = 23. The relative statistical error on the *W** cross-section is 5.4%.

Table 18-16 Cumulative efficiencies for the signal and background processes after each successive cut of the analysis to isolate the W^* process. Also shown are the numbers of selected events after all cuts, for an integrated luminosity of 30 fb^{-1}. The uncertainties listed are due to the Monte Carlo statistics. Note that the number of jets (Njets) includes any *b*-jets.

Description of cuts	Cumulative Selection Efficiency (%)					
	W*	***W-g* fusion**	***Wt***	$t\bar{t}$	$Wb\bar{b}$	***Wjj***
Pre-selection cuts	27.0	20.0	25.5	44.4	2.49	0.667
njets = 2; p_T > 30 GeV	15.7	6.8	3.79	0.93	1.35	0.201
n*b*-jet = 2; p_T > 75 GeV	2.10	0.05	0.018	0.023	0.038	0.0005
scalar sum of p_T >175 GeV	1.92	0.036	0.016	0.021	0.030	0.0004
m_{tot}>200GeV	1.92	0.036	0.014	0.021	0.025	0.0003
150<m_{lvb}<200 GeV	1.67	0.031	0.008	0.017	0.016	0.0002
Events / 30 fb^{-1}	1106 ± 40	510 ± 148	42 ± 21	1290 ± 228	328 ± 61	226 ± 113

18.1.6.6 Determination of V_{tb}

Given the results summarised above, the relative experimental statistical errors on the production cross-sections of the single top processes would be 0.71% for the *W*-gluon process, 2.8% for *Wt* production, and 5.4% for the *W** process. These results imply statistical uncertainties on the extraction of V_{tb} of 0.36% for *W*-gluon fusion, 1.4% for *Wt*, and 2.7% for *W**.

The errors in the extraction of V_{tb} would be dominated by uncertainties in the theoretical predictions of the cross-sections. These arise from uncertainties in the parton distribution functions (PDF), uncertainty in the scale (μ) used in the calculation, and the experimental error on the mass of the top quark. As summarised in Table 18-17, the reliance of the *W*-gluon fusion process on gluon PDFs leads to a higher error than in the *W** channel. However, the *W** cross-section has a greater relative dependence on the top mass. Despite this heightened dependence on the top mass, the overall theoretical error on the cross-section is lowest for *W** (assuming the top mass will be measured to ±2 GeV). For detailed discussions of the theoretical errors, see references [18-50], [18-51], [18-52] and [18-53]. The *Wt* cross-section at the LHC is not currently well known theoretically; the value of 50% quoted in the table reflects the range of values appearing in the literature. The measurement of V_{tb} is also sensitive to errors in the cross-sections of the backgrounds. In particular, the cross-section for the *Wjj* process at the LHC is not well known.

Table 18-17 Relative errors, and their sources, in the cross-sections for single top production. The error due to imprecision in the top mass is quoted assuming δm_t = 2 GeV. For more details, see the text.

Source	δσ/σ (%)		
of Error	***W****	***W-g* fusion**	***Wt***
Statistical	5.4	0.71	2.8
PDF	4	10	-
μ (scale)	4	5	-
δm_t	5	2	-
Total theory error	7.5	11	≈50

Another source of error is due to the kinematic modelling of the signal and backgrounds by the Monte Carlo generators. Rather harsh cuts are required to extract the signals from background, leading to signal efficiencies of typically of 1 - 3%. Extrapolating from the experimentally measured cross-section to the theoretical prediction will introduce additional uncertainty into the extraction of V_{tb}. Also, the only *Wjj* events which contribute to the background are in the far reaches of the tails of the invariant mass and transverse momentum distributions. Since these are extremely unusual events, it is not clear that the simulation is accurate in this regime. This problem of modelling the tails of high rate backgrounds is common among many ATLAS physics analyses and requires further study.

18.1.6.7 Measurements of *W* and top polarisation in *W*-gluon fusion

Single top production provides an opportunity to study the polarisation of top quarks as well as of the *W* bosons produced in their decay. As discussed below, the SM predicts that about 70% of *W* bosons produced in top decay will be longitudinally polarised. Furthermore, in the limit of zero *b*-quark mass, the SM predicts that the top quarks produced in the *W*-gluon fusion process at LO are almost 100% polarised. Since the top decays too quickly to hadronise or depolarize, its spin information is transmitted to its decay products. New physics, such as top production in the decay of a heavy charged Higgs boson or the existence of V+A couplings at the *W-t-b* vertex, could alter the decay angular distributions of either the *W* boson or the top quark. Investigations of the *W* and top polarisations (for more details, see reference [18-54]) are discussed below.

The polarisation of the *W* boson can be investigated through measurements of distributions of its decay products [18-27]. For example, the cosine of the decay angle of the lepton, $\cos_W\Theta_l$, measured in the *W* rest frame with respect to the direction of the *W* boson momentum vector in the top rest frame, can be readily obtained from the *l-b* invariant mass (m_{lb}) as: $\cos_W\Theta_l \cong 2 \cdot m_{lb}^2/(m_t^2 - m_W^2) - 1$. The differential angular distribution can be decomposed into three terms:

$$F_W(\cos_W\Theta_l) = \frac{3}{2} \cdot \left[f_{long} \cdot \left(\frac{\sin_W\Theta_l}{\sqrt{2}} \right)^2 + f_L \cdot \left(\frac{1 - \cos_W\Theta_l}{2} \right)^2 + f_R \cdot \left(\frac{1 + \cos_W\Theta_l}{2} \right)^2 \right]$$

where f_R, f_L and f_{long} are the fractions of right, left and longitudinal components of the *W* polarisation. According to the SM, $f_R = 0$ and $f_{long}/f_L = m_t^2/(2m_W^2)$. With m_t = 175 GeV, the SM predicts $f_{long} = 0.703$ and $f_L = 0.297$.

Events with right-handed *W* polarisation were introduced into the simulation by treating the neutrino in SM events as a charged lepton, and vice versa. In addition to a sample of events simulated with the SM prediction, a ‘SM-like’ scenario, in which the non-longitudinal fraction $1 - f_{long} = 0.297$ is shared by f_R and f_L, was simulated. The simulations were performed at the parton level. As an example, Figure 18-35 shows the distribution of $\cos_W\Theta_l$ for the Standard Model scenario and the more general situation with $f_{long} = f_{long}^{SM} = 0.703$, $f_L = 0.90 \times f_L^{SM} = 0.267$ and $f_R = f_L^{SM} - f_L = 0.030$.

Several functions were used to fit the $\cos_W\Theta_l$ distributions, including a pure SM fit which assumes f_R=0, a ‘SM-like’ fit with f_{long} fixed to the SM value and the fractions f_L and f_R being returned, and a more general fit in which all three components were left free. The results obtained with the SM sample yielded values for f_{long}, f_L and f_R which differed by less than 1.5% from the generated values. When using the mixed sample, the ‘SM-like’ and the more general fit both re-

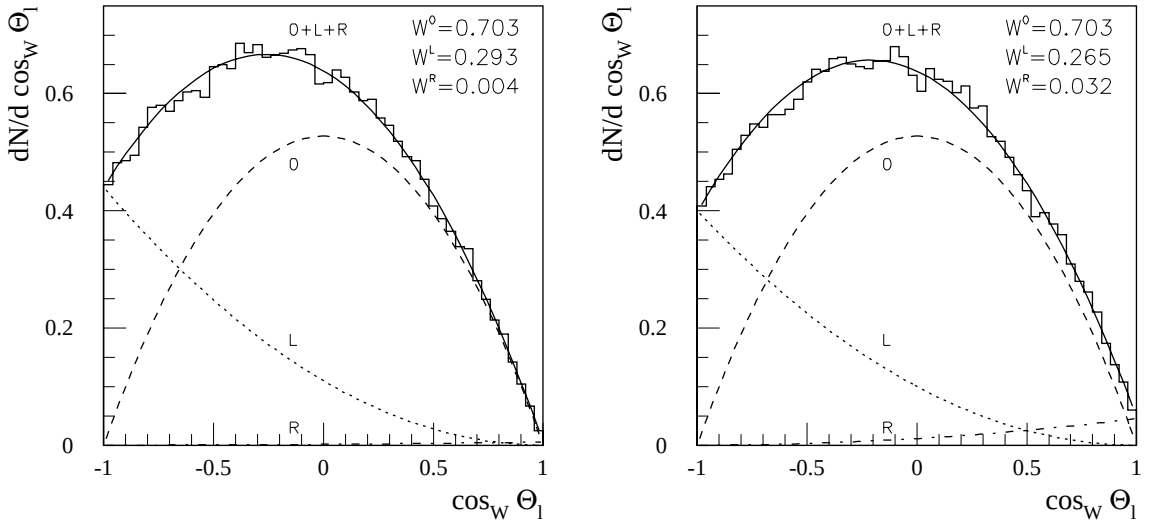

Figure 18-35 Distributions of the cosine of the lepton angle in the W rest frame for the SM scenario with f_R=0, (left figure) and a "SM-like" scenario in which there is a 3% right-handed component included at the expense of the left-handed fraction. The curves correspond to a SM-like fit (f_{long} = 0.703, f_L + f_R = 0.297) resulting in f_R= 0.004 (left) and f_R = 0.032 (right). In each figure, the contributions from longitudinal (O), left-handed (L) and right-handed (R) polarisations are shown separately, as well as their sum.

turned a non-zero value for f_R of ~11% (the 'SM-like' fit results are shown in Figure 18-35). In the non-SM scenario, a pure SM fit under the hypothesis of a zero f_R is clearly disfavoured, with a χ^2 per degree of freedom five times higher than obtained with the fit with f_R as a free parameter.

In addition to measuring the W helicity, the polarisation of the top quarks produced in W-gluon fusion can be observed by measuring the angular distribution of the lepton in the top rest frame with the polarisation axis defined by the direction of the top in the center-of-mass frame of the two incoming quarks. In this frame, the situation is like a 2-2 scattering in electron-positron annihilation. The distribution of $\cos_t\Theta_l$ in this frame is described by

$$F_t(\cos_t\Theta_l) = f_L \cdot \frac{1-\cos_t\Theta_l}{2} + f_R \cdot \frac{1+\cos_t\Theta_l}{2}$$

Unlike the decay scenario, which used a Lorentz invariant to define the angle, a boost is required which introduces a minor skewing of the distribution. Depending on how the neutrino longitudinal momentum is defined, this skewing is more or less pronounced. As can be seen from Figure 18-36, the skewing of the distribution due to the algorithm used to define the boost is minimal. The fits denoted on the figure show the fitted fractions of left- and right-handed components for the helicity of the top quark. Since these are Standard Model distributions, the right handed component is expected to be zero. The fitted RH helicity fractions, reflect the uncertainty from the Monte Carlo statistics. Further study is required to move beyond this parton-level study and to understand the final sensitivity to a right-handed component, including detector effects.

In principle, for polarised top quarks, the asymmetry in the number of events produced with a particular charged lepton into and out of the decay plane should be zero for a T-conserved process. Hence, a non-zero measurement of this asymmetry could be interpreted as evidence for CP-violation, given the assumption of conserved CPT. It has been estimated in the literature [18-27]

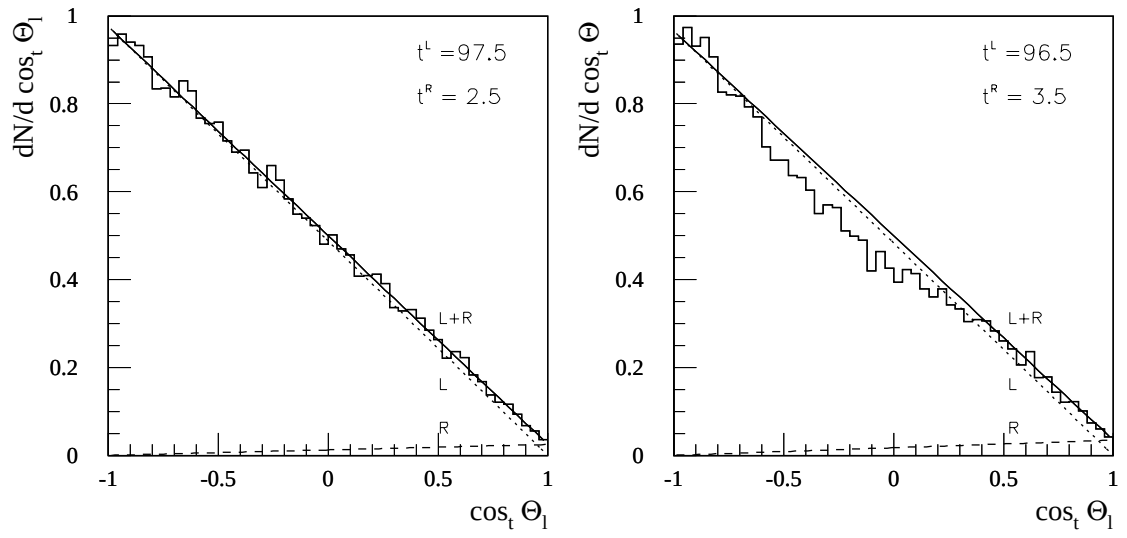

Figure 18-36 Distribution of the cosine of the lepton angle in the top rest frame, reconstructed using the true neutrino momentum (left figure) and using the longitudinal momentum for the neutrino which gives the best top quark mass fit (right figure). Superimposed on each figure are the results of the fit, showing the resulting left-handed (L) and right-handed (R) polarisations separately, as well as their sum.

that approximately 10^7-10^8 single top events would be required to detect CP violation at the level of 0.1-1%. While this is perhaps within reach of the statistics available over the lifetime of the LHC, such a study has not yet been carried out.

18.1.6.8 Conclusions of electroweak single top studies

While further work is required in order to fully understand the detector effects, the initial conclusions are that ATLAS is capable of extending the measurements expected from Fermilab into a new energy regime in which the cross-sections are very large. Backgrounds from $t\bar{t}$ production and W production with heavy flavor appear to be manageable, although detailed measurements of heavy quark production in association with W bosons will be necessary for precise control. Exploiting the three different single top production mechanisms, independent measurements of V_{tb} can be made which will provide both its definitive determination at the statistical level of a fraction of a percent as well as important tests of non-standard physics possibilities. The production of polarised top quarks is a unique feature of its weak production mechanism which will allow for precise helicity measurements at both the production and the decay vertices.

18.1.7 Conclusions of top quark physics studies

The large production cross-sections at the LHC for $t\bar{t}$ pair production and electroweak single top production imply that, in one year of running at low luminosity (10^{33} cm^{-2}s^{-1}), a sample of top quark events will be produced which is more than 10^4 times larger than the data set used at the Fermilab Tevatron to discover the top quark. Over the lifetime of the ATLAS experiment, samples of many millions of top quark events will be selected.

These large data sets will allow very sensitive studies of the properties of the top quark. The mass of the top quark will be measured with a precision of less than 2 GeV, dominated entirely by systematic errors. The top quark Yukawa coupling can be measured with a precision of less than 10% for a Higgs mass of 100 GeV. The $t\bar{t}$ spin correlations predicted in the SM can be observed, and used to probe for anomalous couplings or CP violation. Heavy resonances decaying to $t\bar{t}$ could be detected with masses up to 3 TeV for $\sigma \times$ BR greater than about 10 fb. Rare decays of the top quark can be probed down to branching ratios as low as of order a few times 10^{-5}. Finally, the detailed study of three different mechanisms of electroweak single top production will yield a wealth of information including precision measurements of V_{tb}, measurement of the W and t polarisations, and searches for anomalous couplings.

18.2 Fourth generation quarks

Data from LEP and SLC imply the existence of only three SM families with light neutrinos. However, extra generations with heavy neutrinos are not excluded, and models which include them have been proposed. The current experimental limits on fourth family quarks and leptons are $m_l > 80$ GeV and $m_Q > 128$ GeV [18-29]. The measurement of the ρ parameter [18-29] constrains the mass splitting between the doublet members of possible heavy generations of quarks: $\Sigma_i(c_i/3)\Delta m_i^2 < (49\ \text{GeV})^2, (83\ \text{GeV})^2$, where c_i is the colour factor, and where the first (second) limit corresponds to a Higgs mass of about 90 GeV (300 GeV). Considering only fourth family quarks, an analysis gives $\Delta m = |m(d_4) - m(u_4)| < 43$ GeV (72 GeV).

To take a specific model as an example, the democratic mass matrix (DMM) approach, developed as one possibility for solving the problem of the masses and mixings of the fundamental particles is considered. In the DMM approach, the SM is extended to include a fourth generation of fundamental fermions, with masses typically in the range from 300 to 700 GeV [18-55]. In order to avoid violation of partial wave unitarity, the quark masses should be smaller than about 1 TeV [18-56]. A few efforts have been made to parametrise the CKM matrix to take into account a possible fourth family [18-57][18-58]. These models predict that the fourth generation quark masses are close to each other, and that two-body decays of fourth family quarks are dominant over three-body decays. Guided by these models, two sets of mass values: $m(u_4) \approx m(d_4) \approx 320$ GeV and $m(u_4) \approx m(d_4) \approx 640$ GeV, together with the CKM values in references [18-59] and [18-57] are studied.

A fourth generation of fermions would contribute to the loop-mediated processes in Higgs production ($gg \rightarrow H$) and decay ($H \rightarrow \gamma\gamma$, $H \rightarrow$ gg) [18-61].

This effect would both enhance the Higgs production cross-section, and modify the branching ratios for Higgs decay. Table 18-18 summarises a few examples of the predicted enhancement, relative to the three-generation SM, a fourth generation would give in the values of $\sigma \times \mathrm{BR}$ for the channels $H \to \gamma\gamma$ and $H \to ZZ$. The enhancement is typically a factor of approximately 7-10 for the $H \to ZZ$ (and also $H \to WW$) channels, and up to 2 for $H \to \gamma\gamma$. The enhancements are almost independent of the assumed mass of the fourth family quarks or any other parameters.

Table 18-18 The enhancement, compared to the prediction of the three generation SM, in Higgs production and decay due to a fourth generation of fermions of mass 320 GeV or 640 GeV.

SM	**Enhancement in $\sigma \times$ BR**			
Higgs	**$\sigma \times$ BR($H \to \gamma\gamma$)**		**$\sigma \times$ BR($H \to ZZ$*)**	
Mass (GeV)	**m_4=320 GeV**	**m_4=640 GeV**	**m_4=320 GeV**	**m_4=640 GeV**
120	1.16	1.18	9.79	7.79
130	1.33	1.35	9.46	9.40
150	2.19	2.22	7.36	7.28
170			11.4	11.2
180			8.39	8.23

Of course, as discussed below, more clear evidence for the existence of a fourth generation of quarks could be obtained by searching for them directly. Fourth family quarks would be produced in pairs at the LHC. The expected production cross-section as a function of heavy quark mass was plotted in Figure 18-1, and shows that $\sigma \approx 10$ pb for a quark mass of 400 GeV, decreasing to ≈0.25 pb for a mass of 800 GeV.

18.2.1 Fourth family up quarks

The fourth generation up-type quark (u_4) would predominantly decay via $u_4 \to Wb$. The expected event topologies are thus the same as for $t\bar{t}$ production, except for the different mass of the u_4 quark. The best channel for observing $u_4\bar{u}_4$ production would be the 'single lepton plus jets' mode where one W decays leptonically ($W \to l\nu$) and the other hadronically ($W \to jj$) [18-60].

Events of the topology $u_4\bar{u}_4 \to WWb\bar{b} \to (l\nu)(jj)b\bar{b}$ were generated with PYTHIA and simulated with ATLFAST. Events were selected by requiring $E_{\mathrm{T}}^{\mathrm{miss}} > 20$ GeV and the presence of an isolated electron or muon with $p_{\mathrm{T}} > 50$ GeV and $|\eta| < 2.5$. The lepton isolation criteria required the separation in pseudorapidity / azimuthal angle space between the lepton and any jet to exceed 0.4, and that the total transverse energy deposition in cells within a cone $\Delta R < 0.2$ around the lepton not exceed 10 GeV. Two very hard ($p_{\mathrm{T}} > 250$ GeV) jets were required to be tagged as b-jets. An additional pair of jets, not tagged as b-jets, was required to satisfy 50 GeV $< m_{jj} <$ 100 GeV in order to be loosely consistent with m_W. Accepted W candidates were then combined with the b-tagged jets to search for evidence of $u_4 \to Wb \to jjb$. The mass resolution and efficiency were 21 GeV and 1.1%, respectively, for $m(u_4) = 320$ GeV. For $m(u_4) = 640$ GeV, the corresponding values were 40 GeV and 0.6%.

The background is dominated by $t\bar{t}$ production with subsequent decay $t\bar{t} \to (l\nu)(jj)b\bar{b}$. This background process has the same final state as the signal, as well as a large cross-section. In addition, there are smaller backgrounds from W + 4 jets, WW + 2 jets, and ZZ + 2 jets. The hard kinematic cuts are effective at reducing the backgrounds. The W and WW backgrounds are further suppressed by the requirement of two b-tagged jets. The background from ZZ + 2 jet production, with one Z decaying leptonically and the other to $b\bar{b}$, is very small after cuts.

Table 18-19 presents the expected number of observed events due to $u_4\bar{u}_4$ pair production for different u_4 masses and for an integrated luminosity of 100 fb^{-1}, together with the contributions from the background processes. Figure 18-37 shows the reconstructed m_{jjb} distributions for signal and background in the cases of u_4 quark mass of 320 GeV. In addition to a prominent top quark peak, an excess around the u_4 quark mass is observed.

Table 18-19 For three different u_4 masses, the expected number of selected events for the $u_4\bar{u}_4$ signal and the backgrounds in the single lepton plus jets mode, for an integrated luminosity of 100 fb^{-1}.

	Mass of u_4 quark	
Process	**320 GeV**	**640 GeV**
$u_4\bar{u}_4$ signal	7067	1060
$t\bar{t}$	12880	5953
W + 4 jets	507	218
WW + jj	75	32
ZZ + jj	11	4
Total Background	13473	6207
$S/\sqrt{B}$	61.0	13.5
S/B	0.52	0.17

The corresponding values of $S/\sqrt{B}$ and S/B are also presented in Table 18-19. With an integrated luminosity of 100 fb^{-1}, a u_4 signal could in principle be discovered with greater than 5σ significance for both u_4 masses. However, as $m(u_4)$ increases, the decreasing value of S/B and the increasing width of the signal will make challenging the task of extracting the signal above background. An investigation is underway of the possibility to further improve extraction of the signal by simultaneously reconstructing the $u_4 \rightarrow$ lvb decay, and requiring that both decays give the same u_4 mass.

Events of the 'all jets' topology $u_4\bar{u}_4 \rightarrow WWb\bar{b} \rightarrow (jj)(jj)b\bar{b}$ with both W bosons decaying hadronically have also been studied [18-62]. The signature for this channel is characterised by six or more jets in the final state. QCD multi-jet events are the dominant source of background, with an estimated cross-section of about 5.5 μb. Other backgrounds sources include $t\bar{t}$ and W plus jet production.

In addition to the two very hard b-jets ($p_T > 250$ GeV) required above, the selection criteria demanded at least 6 jets with $p_T > 20$ GeV (including the two tagged b-jets) and no isolated lepton in the final state. Table 18-20 shows the number of generated signal and background events before and after applying these event selection cuts, and illustrates the effectiveness of the cuts in very significantly decreasing the backgrounds from QCD multi-jets and W+jets production.

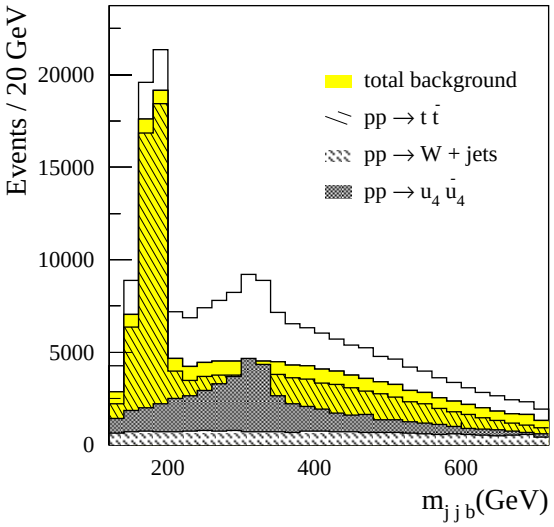

Figure 18-37 Invariant m_{jjb} mass distribution for selected single lepton plus jet events for $m(u_4)$ = 320 GeV, normalised to an integrated luminosity of 100 fb^{-1}.

The $W \rightarrow jj$ decay was reconstructed from the light quark jets. The combinations satisfying $|m_{jj} - m_W| < 15$ GeV were then combined with all b-tagged jets. Further background reduction was achieved by requiring $H_T > 500$ GeV, where H_T is defined as the scalar sum of the transverse energies of all the reconstructed jets. The resulting m_{jjb} mass resolution and signal efficiency were 22 GeV and 6.9%, respectively, for $m(u_4)$ = 320 GeV. The corresponding values for $m(u_4)$ = 640 GeV were 36 GeV and 0.4%.

Table 18-20 All jets $u_4\bar{u}_4$ signal and background event samples, before and after applying the selection cuts.

Process	Evts generated	Evts after cuts
$u_4\bar{u}_4$ Signal	$2.0 \cdot 10^6$	$6.8 \cdot 10^5$
QCD jets	$2.0 \cdot 10^8$	$3.9 \cdot 10^4$
$t\bar{t}$	10^7	$1.4 \cdot 10^6$
W + jets	$1.0 \cdot 10^8$	10^4

Table 18-21 summarizes the number of signal and background events surviving these cuts. It is clear from the small S/B values that the backgrounds from QCD and from $t\bar{t}$ dominate over the signal. The QCD background is of particular concern, since its cross-section at the LHC is not well known. The rather broad m_{jjb} signal distribution, due to the many different combinations possible, also complicates efforts to extract the signal above background. For u_4 masses which are not too high, it is possible that the all-jets analysis could be used to support a discovery made in the single lepton plus jets decay channel.

Table 18-21 Expected rates of the fourth family up-quarks in all-jets mode and various backgrounds for an integrated luminosity of 100 fb^{-1}.

	Mass of u_4	
Process	**320 GeV**	**640 GeV**
$u_4\bar{u}_4$ signal	96.8k	2390
QCD multi-jets	491k	144k
$t\bar{t}$	296k	64k
W + jets	17.6k	7.2k
Total Bkgnd	804.6k	215.2k
S/B	0.12	0.01

18.2.2 Fourth family down quarks

Under the assumption that $m(d_4) \approx m(u_4)$, the dominant d_4 decay mode would be $d_4 \rightarrow tW^-$. The most promising final state to search for $d_4\bar{d}_4$ pair production is the single lepton plus jets channel $pp \rightarrow d_4\bar{d}_4 \rightarrow t\bar{t}W^+W^- \rightarrow W^+bW^-\bar{b}W^+W^-$, where one of the W decays leptonically and the others decay hadronically [18-62]. The dominant background for this channel is $t\bar{t}$ production with additional jets. Other sources of background, such as WW+jets and W+jets, do not contribute significantly.

Events satisfying the final state topology $d_4\bar{d}_4 \rightarrow l + 2b_{\text{jet}} + 6j + E_T^{\text{miss}}$ were required to have exactly eight jets with $p_T > 20$ GeV, including two b-tagged jets, and one isolated electron or muon with $p_T > 20$ GeV. In addition, a requirement was imposed that $E_T^{\text{miss}} > 20$ GeV. Di-jet pairs satisfying $|m_{jj} - m_W| < 15$ GeV were considered as $W \rightarrow jj$ candidates, and were combined with b-tagged jets to search for $t \rightarrow jjb$ candidates. Combinations with $|m_{jjb} - m_t| < 15$ GeV were considered as top quark candidates. Finally, $t \rightarrow jjb$ and $W \rightarrow jj$ candidates were combined to search for a signal from the hadronic decay $d_4 \rightarrow tW \rightarrow (jjb)jj$. The resulting mass resolution was 42 GeV, with a signal efficiency of 0.54%.

Figure 18-38 shows the invariant mass distributions of the (*jjb*)*jj* system for the signal and $t\bar{t}$ background in the case $m(d_4)$ = 320 GeV, assuming an integrated luminosity of 100 fb^{-1}. Within a mass window of 320 ± 60 GeV, a total of about 29 400 signal events were selected, with a background of about 39 000 events. The d_4 signal and $t\bar{t}$ background shapes are very similar. However, the size of the excess is much larger than the uncertainty in the knowledge of the $t\bar{t}$ cross-section. Observation of such an excess would be a clear signal of new physics, though further studies would be required to determine the cause of the enhancement. For the case with $m(d_4)$ = 640 GeV and an integrated luminosity of 100 fb^{-1}, 2 043 signal events would be accepted, with a background of 3 479 events in the mass interval 640 ± 75 GeV. The very broad signal shape would complicate detection of the signal above background.

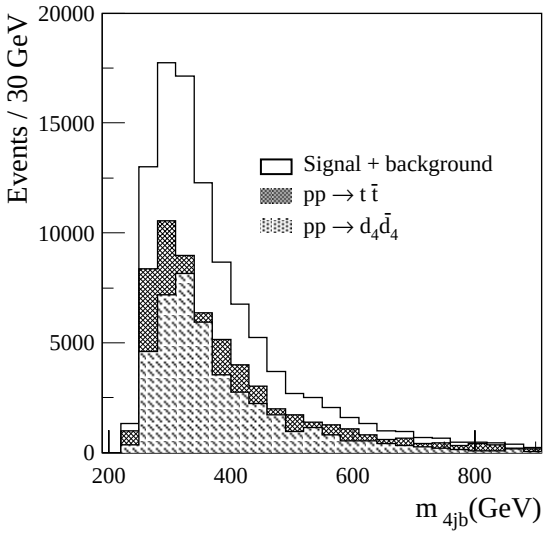

Figure 18-38 Invariant mass distribution of the *(jjb)jj* system for $m(d_4)$ = 320 GeV, normalised to an integrated luminosity of 100 fb^{-1}.

These results can be improved by more fully utilising the knowledge of the final state, and the resulting kinematic constraints (such as m_W and m_t constraints for the appropriate combinations). It has been shown in the analysis of $t\bar{t}H$ for example (see Section 19.2.4.3), that it is possible to simultaneously reconstruct both top quark decays, thereby reducing greatly the number of possible combinations. Application of such techniques here should improve the separation of the signal from background, and are being studied.

18.2.3 Bound states of fourth family quarks

If the decays of fourth generation quarks were suppressed, for example due to small inter-generation mixings, the resultant long quark lifetime could lead to formation of a $Q_4\overline{Q}_4$ bound state [18-63] such as a pseudoscalar quarkonium state η_4. As already said, the extension of the DMM model to include a fourth family predicts a mass difference between u_4 and d_4 of the order of 1 GeV. Given the expected experimental resolution of ATLAS, this mass difference would not allow the identification of the quark type which compose the quarkonium.

The production of a superheavy quarkonium via $gg \rightarrow \eta_4$ process has been implemented in PYTHIA. The decay $\eta_4 \rightarrow ZH$, followed by $Z \rightarrow ll$ and $H \rightarrow b\bar{b}$, has been studied [18-65] for $m(\eta_4)$ = 600 GeV and m_H = 150 GeV assuming $\sigma \times \mathrm{BR}$ = 0.19 pb (including BR($Z \rightarrow ll$) and BR($H \rightarrow b\bar{b}$)). The main background for this channel is due to Z+jets production ($\sigma \sim 1.7\times10^4$ pb). Continuum ZH production does not contribute significantly ($\sigma \sim 6\text{x}10^{-3}$ pb).

The selection cuts required the presence of two isolated opposite-sign, same-flavour leptons with $p_T > 20$ GeV and satisfying $|m_{ll} - m_Z| < 10$ GeV. In addition, two jets with $p_T > 15$ GeV were required to be tagged as *b*-jets. Evidence for the decay $\eta_4 \rightarrow ZH$ was then searched for by reconstructing the $llb\bar{b}$ invariant mass. The resulting mass resolution was 25 GeV, with a signal efficiency of 7%.

As shown in Figure 18-39, a clear signal of $\eta_4 \rightarrow ZH$ can be seen near the mass $m(\eta_4)$ = 600 GeV. With an integrated luminosity of 100 fb^{-1}, the estimated number of signal and background events are 4660 and 573 events, respectively.

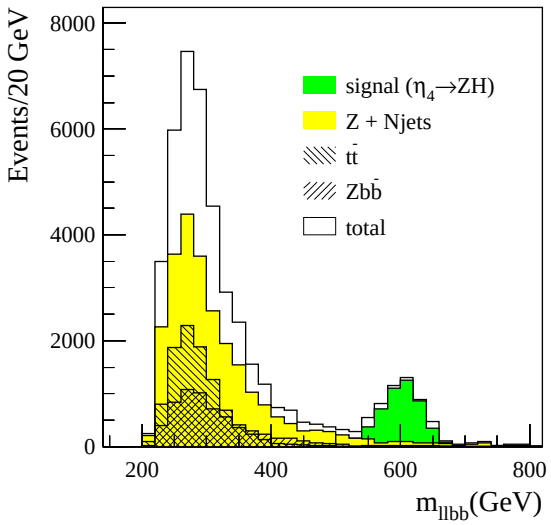

Figure 18-39 The $llb\bar{b}$ invariant mass distribution for the $\eta_4 \rightarrow ZH$ signal and background, normalised to an integrated luminosity of 100 fb^{-1}.

18.3 Heavy leptons

Accurate measurement of the parameters of Z decay have demonstrated that there exist only three light neutrinos coupling to the Z with SM couplings. The simplest supposition is then that the lepton sector comprises these three light neutrinos and their charged counterparts. However, it is quite possible that heavy leptons exist.

Many models, such as composite models [18-66], left-right symmetric models [18-67], grand unified theories [18-68], technicolor models [18-69], superstring-inspired models [18-70], and models of mirror fermions [18-71], predict the existence of new particles with masses around of the scale of 1 TeV and allow the possible existence of new generations of fermions. For illustration purposes, the case of heavy, 'fourth generation' leptons which have SM couplings is considered. In this case, production of a pair of heavy charged leptons (LL) or a pair of heavy neutrinos ($N\overline{N}$) at the LHC is dominated by the Drell-Yan process and by gluon-gluon fusion. The total production cross-section, $\sigma(LL)$, is of order 1 pb at the LHC for $m_L \approx 100$ GeV, decreasing to a few fb for $m_L \approx 700$ GeV, with similar predictions for $N\overline{N}$ production [18-72].

The experimental signatures for detection of these heavy leptons depends critically on their masses and decay modes. Searches for $L \rightarrow NW$ have been discussed in the literature [18-73], and have concluded that it would be very difficult to separate the signal from the large backgrounds from single and pair production of W and Z bosons. However, these analyses were performed with the assumption of a massless fourth-generation neutrino, and need to be repeated for a massive neutrino. In addition to this approach, the case where both the L and the N are massive gives rise to other possibilities. For example, if the L and N were roughly degenerate, the decay $L \rightarrow NW$ (and $N \rightarrow LW$) would be kinematically forbidden. Instead, the heavy leptons would decay predominantly through their mixing with the light lepton generations. In this case, the charged lepton decay $L \rightarrow \nu W$ could be suppressed by a small mixing angle so that the L could be relatively long-lived and would look like a muon escaping the detector. However, due to its large mass, the velocity distribution for L production would not be peaked as sharply at $\beta \approx 1$ as for muon production. Measurement of its time-of-flight with the muon spectrometer could then be used to identify and determine the mass of the heavy charged lepton. Such an analysis is reported in Section 20.3, where the situation with heavy long-lived charged sleptons was examined in the context of gauge-mediated supersymmetry breaking models. In the case where the decay $N \rightarrow lW$ (with l a light lepton) occurs inside the detector, an interesting signature of $N\overline{N} \rightarrow llWW$ production would be the production of high p_T lepton pairs in association with jets (for the case where both W bosons decay hadronically). The dominant background, arising from $t\bar{t}$ production, could be suppressed by requiring no E_T^{miss} and by trying to recon-

struct the N mass from ljj combinations. The cases of $pp \rightarrow N\overline{N} \rightarrow lljjjj$ and $pp \rightarrow e\overline{N} \rightarrow eejj$ in left-right symmetric models are presented in Section 21.6.2. Studies are underway of the ATLAS sensitivity to these and other possible experimental signatures of heavy lepton production.

18.4 Conclusions

The LHC, with its high beam energy and luminosity, will be an excellent place to search for, and explore the properties of, heavy quarks and leptons. The cross-section for $t\bar{t}$ production at the LHC is about 100 times larger than that at the Tevatron, and will lead to accumulation over the lifetime of ATLAS of millions of $t\bar{t}$ events. Studies of these events, and the large samples of electroweak single top quark events, will permit very detailed studies of the properties of the top quark, and will allow sensitive probes of the EWSB sector. In addition, the existence of fourth generation quarks will be probed for masses up to of order 700 GeV. A great discovery potential, not yet fully evaluated, also exists for heavy leptons.

18.5 References

18-1 R. Bonciani *et al.*, Nucl. Phys. **B529** (1998) 424.

18-2 E. Richter-Was, D. Froidevaux and L. Poggioli, 'ATLFAST 2.0 a fast simulation package for ATLAS', ATLAS Internal Note ATL-PHYS-98-131 (1998).

18-3 CDF Collaboration, Phys. Rev. **D50** (1994) 2966; Phys. Rev. **D51** (1995) 4623; Phys. Rev. Lett. **74** (1995) 2626.

18-4 D0 Collaboration, Phys. Rev. Lett. **74** (1995) 2422.

18-5 T. Sjostrand, Computer Physics Communications **82** (1994) 74.

18-6 G. Marchesini *et al*, Computer Phys. Commun. 67 (1992) 465.

18-7 Lj. Simic, G. Skoro and D. Popovic, 'Signal and background study for $t\bar{t}$ all hadronic decay at the LHC', ATLAS Internal Note ATL-COM-PHYS-99-057 (1999).

18-8 F.A. Berends and H. Kuijf, Nucl. Phys. **B353** (1991) 59.

18-9 E. Richter-Was and D. Froidevaux, 'MSSM Higgs searches in multi *b*-jets final states', ATLAS Internal Note ATL-PHYS-No-104 (1997).

18-10 K. Sliwa, 'Top mass and cross-section results from CDF and D0 at the Fermilab Tevatron', FERMILAB-CONF-99/086-E. Proceedings of the 13th Topical Conference on Hadron Collider Physics, Tata Institute of Fundamental Research, Mumbai, India (1999).

18-11 U. Sarid, 'Precision top mass measurements vs. Yukawa unification predictions', hep-ph/9610341.

18-12 CDF Collaboration, Phys. Rev. Lett. **80** (1998) 2767;
D0 Collaboration, Phys. Rev. **D58** (1998) 052001.

18-13 P. Grenier *et al.*, 'Measurement of the top quark mass in the inclusive single lepton plus jets channel', ATLAS Internal Note ATL-COM-PHYS-99-024 (1999).

18-14 C. Peterson *et al.*, Phys. Rev. **D27 (**1983) 105.

18-15 ALEPH Collaboration, Phys. Rep. **294** (1998) 1.

18-16 I. Efthymiopoulos, 'High p_T top mass reconstruction in the single lepton plus jets channel using a large calorimeter cluster', ATLAS Internal Note ATL-COM-PHYS-99-050 (1999).

18-17 A. Lagatta, L. La Rotonda and M. Cobal, 'Top mass evaluation in the $t\bar{t}$ dilepton channel', ATLAS Internal Note ATL-COM-PHYS-99-044 (1999).

18-18 G. Unal and L. Fayard, Proceedings of the Large Hadron Collider Workshop, Aachen, 1990, edited by G. Jarlskog and D. Rein, Volume II, p. 360.

18-19 K.J.F. Gaemers and G. Hoogeveen, Phys Lett. **146B** (1984) 347;
D. Dicus, A. Stange and S. Willenbrock, Phys. Lett. **B333** (1994) 126.

18-20 K. Lane and E. Eichten, Phys. Lett. **B352** (1995) 382;
E. Eichten and K. Lane, Phys. Lett. **B327** (1994) 129.

18-21 C.T. Hill and S.J. Parke, Phys. Rev. **D49 (**1994) 4454.

18-22 R. Casalbuoni *et al.*, Z. Phys. **C69** (1996) 519.

18-23 C.T. Hill, Phys. Lett. **B266** (1991) 419; Phys. Lett. **B345** (1995) 483.

18-24 E. Simmons, Phys. Rev. **D55 (**1997) 1678.

18-25 N. Cartiglia and J. Parsons, 'Study of ATLAS sensitivity to a heavy resonance decaying to $t\bar{t}$', ATLAS Internal Note ATL-COM-PHYS-99-038 (1999).

18-26 G. Mahlon and S. Parke, Phys. Rev. **D53** (1996) 4886.

18-27 G.L. Kane, G.A. Ladinsky and C.-P. Yuan, Phys. Rev. **D45** (1992) 124;
W. Bernreuther and. A. Brandenburg, Phys. Rev. **D49** (1994) 4481;
C.-P. Yuan, Mod. Phys. Lett. **A10** (1995) 627;
W. Bernreuther and A. Brandenburg, Phys. Lett. **B314** (1993)104.

18-28 A. Lagatta, V. Simak and J. Smolik, '$t\bar{t}$ spin correlations and the potential for observation of CP violation in the production vertex', ATLAS Internal Note ATL-COM-PHYS-99-049 (1999).

18-29 Particle Data Group, Review of Particle Physics, European Physical Journal **C3** (1998) 1.

18-30 J. Konigsberg, FERMILAB-CONF-99/129-E. Published Proceeding, 17th International Workshop on Weak Interactions and Neutrinos (WIN 99), Cape Town, South Africa, 1999.

18-31 B. Grzadkowski, J.F. Gunion, and P. Krawczyk, Phys. Lett. **B268** (1991) 106;
G. Eilam, J.L Hewett, and A. Soni, Phys. Rev. **D44** (1991) 1473;
M. Luke and M.J Savage, Phys. Lett. **B307** (1993) 387.

18-32 C.S Li, R.J Oakes, and J.M. Yang, Phys. Rev. **D49** (1994) 293;
J.M. Yang and C.S. Li, Phys. Rev. **D49** (1994) 3412;
G. Couture, C. Hamzaoui, and H. Koenig, Phys. Rev. **D52** (1995) 1713;
G. Couture, M. Frank, and H. Koenig, Phys. Rev. **D56** (1997) 4219;
G.M. de Divitiis, R. Petronzio, and L. Silvestrini, Nucl. Phys. **B504** (1997) 45.

18-33 R.D. Peccei and X. Zhang, Nucl. Phys. **B337** (1990) 269;
T. Han, R.D. Peccei, and X. Zhang, Nucl. Phys. **B454** (1995) 527;
T. Han *et al.*, Phys. Lett. **B385** (1996) 311;
M. Hosch, K. Whisnant, and B.L. Young, Phys. Rev. **D56** (1997) 5725;
V.F. Obraztsov, S.R. Slabospitsky, and O.P. Yushchenko, Phys. Lett. **B426** (1998) 393;
T. Han *et al.*, Phys. Rev. **D58** (1998) 73008;
B.A. Arbuzov and M. Y. Osipov, Phys. Atom. Nucl. **62** (1999) 495.

18-34 CDF Collaboration, Phys. Rev. Lett. **80** (1998) 2525.

18-35 L.D. Chikovani and T.D. Djobava, 'ATLAS sensitivity to the flavor-changing neutral current decay $t \rightarrow Zq$', ATLAS Internal Note ATL-COM-PHYS-99-034 (1999).

18-36 J. Dodd, S. McGrath and J. Parsons, 'Study of ATLAS sensitivity to rare top quark decays', ATLAS Internal Note ATL-COM-PHYS-99-039 (1999).

18-37 Y.P. Gouz and S.R. Slabospitsky, 'Double top production at hadron colliders', hep-ph/9811330.

18-38 E. Jenkins, Phys. Rev. **D56** (1997) 458.

18-39 G. Mahlon and S. Parke, Phys. Lett. **B347** (1995) 394;
G. Mahlon, 'Theoretical expectations in radiative top decays', hep-ph/9810485.

18-40 M. Jarabek and J.H. Kuhn, Phys. Lett. **B329** (1994) 317.

18-41 W.G.H. Dharmaratna and G. R. Goldstein, Phys. Rev. **D41** (1991) 1731.

18-42 B. Grzadkowski and J.F. Gunion, Phys. Lett. B287 (1992) 237.

18-43 A.P. Heinson, A.S. Belyaev, and E.E. Boos, Phys., Rev. D56 (1997) 3114.

18-44 V. Barger, J. Ohnemus and R.J.N. Phillips, Int. Journ. Mod. Phys. **A4** (1989) 617.

18-45 E. Malkawi and T. Tait, Phys. Rev. **D54** (1996) 5758;
T. Han et al, Phys. Rev. **D58** (1998) 073008.

18-46 D.O. Carlson, E. Malkawi and C.P. Yuan, Phys. Lett. **B337** (1994) 145;
D.O. Carlson, Ph.D. Thesis, Michigan State University (1995);
Tim Tait, Ph.D. Thesis, Michigan State University (1999).

18-47 SGMP is provided via private communication with authors at Protvino and is not currently publicly available.

18-48 S. Mrenna, T. Tait, C.P. Yuan, private communication.

18-49 D. O'Neil, B. Gonzalez-Pineiro and M. Lefebvre, 'Measuring V_{tb} via s-channel single top production with ATLAS', ATLAS Internal Note ATL-COM-PHYS-99-015 (1999).

18-50 S. Willenbrock, 'Overview of Single Top Theory - Measuring the Cross-section, Theoretical Uncertainties, $|V_{tb}|$, etc.', Talk presented at the 'Thinkshop, top quark Physics for Run II' at Fermi National Laboratory, Bhatavia, Illinois (1998).

18-51 M.C. Smith and S. Willenbrock, Phys. Rev. **D54** (1996) 6696.

18-52 T. Tait and C.P. Yuan, 'Single top production at the Fermilab tevatron', hep-ph/9710372.

18-53 J. Huston et al., Phys. Rev. **D58** (1998) 114034.

18-54 B. Gonzalez-Pineiro et al., 'Top and W polarization in electroweak top production at the LHC', ATLAS Internal Note ATL-COM-PHYS-99-027 (1999).

18-55 A. Celikel, A.K. Ciftci and S. Sultansoy, Phys. Lett. **B342** (1995) 257.

18-56 M.S. Chanowitz, M.A. Furman and I. Hinchliffe, Nucl. Phys. **B153** (1979) 402.

18-57 S. Atag *et al.*, Phys. Rev. **D54** (1996) 5745.

18-58 A. Datta and S. Raychaudhuri, Phys. Rev. **D49** (1994) 4762.

18-59 E. Arik *et al.*, 'A search for fourth family quarks at hadron colliders', ATLAS Internal Note ATL-PHYS-96-091 (1996).

18-60 E. Arik *et al.*, Phys. Rev. **D58** (1998) 117701.

18-61 E. Arik *et al.*, 'Enhancement of the Standard Model Higgs boson production cross-section with a fourth family of Standard Model quarks', ATLAS Internal Note ATL-PHYS-98-125 (1998).

18-62 E. Arik *et al.*, 'Observability of Standard Model fourth family quarks at the LHC', ATLAS Internal Note ATL-PHYS-99-005 (1999).

18-63 V. Barger *et al.*, Phys. ReV. **D35** (1987) 11.

18-64 H. Inzawa and T. Morii, Phys. Lett. **B70** (1993) 20.

18-65 E. Arik *et al.*, 'Production and decay properties of the pseudoscalar quarkonium associated with a fourth generation quark', ATLAS Internal Note ATL-PHYS-99-061 (1999).

18-66 L. Abbot and E. Farhi, Phys. Lett. **101B** (1981) 69; Nucl. Phys. **B189** (1981) 547;
W. Buchmueller, Acta Phys. Austriaca Suppl. XXVII (1985) 517.

18-67 J.C. Pati and A.Salam, Phys. Rev. **D10** (1974) 275;
R.N. Mohapatra and J.C. Pati, Phys. Rev. **D11** (1975) 566 and Phys. Rev. **D11** (1975) 2558;
G. Senjanovic and R.N. Mohapatra, Phys. Rev. **D12** (1975) 1502;
G. Senjanovic, Nucl. Phys. **B153** (1979) 334.

18-68 See, for example, P. Langacker, Phys. Rep. **72** (1981) 185.

18-69 S. Dimopoulos, Nucl. Phys. **B168** (1981) 69;
E. Farhi and L. Susskind, Phys. Rev. **D20** (1979) 3404;
J. Ellis *et al.*, Nucl. Phys. **B182** (1981) 529.

18-70 J.L. Hewett and T.G. Rizzo, Phys. Rep. **183** (1989) 193.

18-71 J. Maalampi, K. Mursula and M. Roos, Nucl. Phys. **B207** (1982) 233.

18-72 See for example P.H. Frampton *et. al.*, Phys. Rev. **D48** (1993) 3128 and references therein.

18-73 See for example V. Barger, T. Han and J. Ohnemus, Phys. Rev. **D37** (1988) 1174, and references therein.